REPORT DOCUMENTATION PAGE

Form Approved
OMB No. 0704-0188

1. REPORT DATE *(DD-MM-YYYY)*	2. REPORT TYPE	3. DATES COVERED *(From - To)*
31-12-2005	Final Technical Report	January, 2005-December, 2005

4. TITLE AND SUBTITLE
High Frequency Guided Wave Phased Array Focusing in Pipe

5a. CONTRACT NUMBER

5b. GRANT NUMBER
N00014-04-1-0092

5c. PROGRAM ELEMENT NUMBER

6. AUTHOR(S)
Rose, Joseph L.
Zhang, Li

5d. PROJECT NUMBER

5e. TASK NUMBER

5f. WORK UNIT NUMBER

7. PERFORMING ORGANIZATION NAME(S) AND ADDRESS(ES)
The Pennsylvania State University
Department of Engineering Science & Mechanics
212 Earth-Engineering Science Bldg.
University Park, PA 16802

8. PERFORMING ORGANIZATION REPORT NUMBER

9. SPONSORING/MONITORING AGENCY NAME(S) AND ADDRESS(ES)
Office of Naval Research Regional
Office Chicago
230 South Dearborn, Rom 380
Chicago, IL 60604-1595

10. SPONSOR/MONITOR'S ACRONYM(S)
ONR

11. SPONSOR/MONITOR'S REPORT NUMBER(S)

12. DISTRIBUTION/AVAILABILITY STATEMENT
Approved for Public Release; distribution is Unlimited

13. SUPPLEMENTARY NOTES

14. ABSTRACT

Ultrasonic non-destructive evaluation is used in industry because of its excellent defect detection potential. Long range ultrasonic guided waves have intrigued investigators for years because of an ability to test structures over a long distance from a single sensor position. Guided waves have much more complex wave behavior than bulk waves in infinite media. The Lamb type guided waves in hollow cylinders spread out and wrap around the circumference when propagating in an axial direction.

Focusing at a certain point in a hollow cylinder is implemented by utilizing the non-axisymmetric energy distributions of flexural wave modes. There are two types of focusing in pipes: natural focusing and phased array focusing. When a partially loaded excitation is used to generate guided waves in cylindrical shells, the excited flexural modes lead to ultrasonic energy naturally focused at certain positions. This special natural focusing phenomenon can be used to improve guided wave inspection results in hollow cylinders.

By applying input time delays and amplitudes for a multi-channel ultrasonic signal generation system, one can focus the guided waves at a pre-selected position. The input parameters of the ultrasonic phased array are calculated by implementing a deconvolution computation of the displacement angular profiles excited by one excitation channel.

Theoretical and experimental results show the power of focusing in the long range ultrasonic guided wave inspection of pipe. Excellent results and superb inspection potential are shown.

15. SUBJECT TERMS
natural focusing, phased array focusing, ultrasonic guided waves, pipe inspection, flexural modes

16. SECURITY CLASSIFICATION OF:			17. LIMITATION OF ABSTRACT	18. NUMBER OF PAGES	19a. NAME OF RESPONSIBLE PERSON
a. REPORT	b. ABSTRACT	c. THIS PAGE		53	Joseph L. Rose
					19b. TELEPHONE NUMBER *(Include area code)* 814-863-8026

A Final Report

On

"High Frequency Guided Wave Phased Array Focusing in Pipe"
(Award # N00014-04-1-0092)
Second Year of Study

Submitted to

Defense Technical Information Center
8725 John J Kingman Road Ste 0944
Fort Belvoir , VA 22060-6218

By

Joseph L. Rose
Li Zhang
Ultrasonic Research and Development
The Penn State University
212 Earth-Engineering Sciences Bldg.
University Park, PA 16802
814-863-8026
jlresm@engr.psu.edu

on

December 31, 2005

ABSTRACT

Ultrasonic non-destructive evaluation is generally used in industry because of its excellent defect detection potential. The ultrasonic waves propagating in a bounded waveguide are called guided waves. Long range ultrasonic guided waves have intrigued investigators for years because of an ability to test structures over a long distance from a single sensor position. Guided waves have much more complex wave behavior than bulk waves in infinite media. Plane-strain guided waves in a single layer plate with traction free boundaries are Lamb waves. The Lamb type guided waves in hollow cylinders spread out and wrap around the circumference when propagating in an axial direction. Therefore, except for the guided waves with axisymmetric energy distributions in a tube, there are an infinite number of non-axisymmetric wave modes called flexural modes that have similar particle behavior as the axisymmetric mode in the same group.

Focusing at a certain point in a hollow cylinder is implemented by utilizing the non-axisymmetric energy distributions of flexural wave modes. There are two types of focusing in pipes: natural focusing and phased array focusing. When a partially loaded excitation is used to generate guided waves in cylindrical shells, the excited flexural modes lead to ultrasonic energy naturally focused at certain positions. This special natural focusing phenomenon can be used to improve guided wave inspection results in hollow cylinders.

By applying input time delays and amplitudes for a multi-channel ultrasonic signal generation system, one can focus the guided waves at a pre-selected position. The input parameters of the ultrasonic phased array are calculated by implementing a deconvolution computation of the displacement angular profiles excited by one excitation channel. Because the angular profiles of the circumferential displacement distributions in a hollow cylinder are decided by the excitation sources, focusing results are strongly affected by the excitation conditions.

A source influence for focusing potential in pipes must be considered. Research shows that excitation focusing potential in hollow cylinders depends highly on the frequencies and sizes of the excitation transducers. An infinitely long transducer along the axis only generates axisymmetric guided waves, although a short axial transducer length has little influence on the focusing results. A transducer with a small circumferential length usually leads to drastic variations of energy distributions in the circumferential direction. If a low frequency guided wave group propagates in a pipe with a small diameter, the flexural modes may be cut-off or have much different velocities from the axisymmetric mode. A single axisymmetric mode can never achieve focusing. Hence, contour charts of focusing potential at different frequencies and with various circumferential excitation lengths are used as directories of the focusing procedures.

Theoretical and experimental results show the power of focusing in the long range ultrasonic guided wave inspection of pipe. Therefore, the research of focusing potential in hollow cylinders becomes a significant achievement for applying pipeline integrity evaluations.

TABLE OF CONTENTS

LIST OF FIGURES

LIST OF TABLES

SECTION 1

INTRODUCTION

1.1 The Problem Statement

Ultrasonic non-destructive testing (NDT) techniques are developed as a practical tool for evaluating the quality and possible failure of structures. The NDT inspection of a structure is carried out by examining ultrasonic wave propagation in the structure and subsequent wave reflections and transmissions. Therefore, a study of the characteristics of ultrasonic waves in various geometrical waveguides and materials becomes quite indispensable.

Ultrasonic waves can be bulk waves or guided waves. Bulk waves are waves traveling in infinite media; guided waves, such as Lamb waves, surface waves, and interface waves, that exist only in bounded waveguides. The guided waves propagating in hollow cylindrical waveguides (or pipes) are investigated in this work. Due to their excellent defect detection sensitivity and ability for propagating long distances, ultrasonic guided waves have been increasingly used in many industrial applications including nondestructive evaluation [1]. All characteristics of guided waves, such as guided wave dispersion, wave structure, source influence and numerous simulations, are summarized by Zhang (2005) [2].

Based upon the research results from Gazis (1959) [3, 4] and Ditri and Rose (1992) [5], Li and Rose developed an analytical method to simulate the energy distribution in the circumferential direction (known as angular profiles) in hollow cylinders [6], in 2002, where they presented the phased array focusing technique for longitudinal guided waves propagating in cylindrical shells [7]. Sun et al carried out the angular profile calculations and the phased array focusing technique for torsional guided wave propagation in hollow cylinders [8-10]. If the angular profiles show that ultrasonic energy is naturally concentrated at a circumferential location at a particular propagation distance, this phenomenon is called "natural focusing" [16, 17]. The natural focusing phenomenon can also be used to improve guided wave inspection.

Phased array focusing is not always achievable over a certain frequency range. Many factors that influence the focusing results must be considered before applying the phased array focusing. For example, the various sizes of the ultrasonic wave generators change both the energy distributions in the radial direction (known as wave structures) and the angular profiles of a particular mode group. Some geometry and material inhomogeneities could also alter the energy distributions in a pipe leading to a failure of the focusing technique.

In this work, the focusing potential of guided waves in hollow cylinders with variable geometries and/or material properties is investigated. Guided waves are generated by applying different excitation conditions and subsequent propagation in hollow cylinders with various geometries, such as welds and elbows [11-13]. In addition, the potential of inspecting a hollow cylinder by applying a frequency and angle tuning (FAT) natural focusing technique is also discussed [14-17].

1.2 Analytical Calculations of Guided Waves in Hollow Cylinders

In the 1880's, researchers began a study of many elastic wave propagation problems. Lord Rayleigh and Lamb investigated the wave propagations in a single-layer elastic isotropic plate with traction free boundary conditions [18, 19]. Their work led to the Rayleigh-Lamb frequency equation (Equation A.1), which describes a dispersion relationship between the frequency and the wave number of an elastic wave.

In 1923, Ghosh obtained the first mathematical solution for the longitudinal, axisymmetric mode wave propagation in a hollow cylinder [20], although for a special case of a rod with co-axial cannulas. Love (1944) and Rayleigh (1945) generally studied elastic wave propagation in hollow cylinders by using shell theory [18, 21]. Various improvements for the analysis of wave propagation in cylindrical waveguides were presented by McFadden [22], Naghdi and Cooper [23], Lin and Morgan [24], and Mirsky and Herrmann [25, 26]. Especially, Mirsky and Herrmann brought forward shear deformation effects and flexural, rotary inertia in shell analysis. However, all of the earlier research was based on an assumption of axisymmetric wave motion in hollow cylinders.

Approximate solutions for non-axisymmetric wave propagation in cylindrical shells were presented by Cooper and Naghdi in 1957 [27]. Based on Mirsky and Herrmann's enhanced shell analysis, D. C. Gazis obtained the first exact solution to the propagation of harmonic guided waves in an infinite circular hollow cylinder in 1959 [3, 4]. The solution treats completely axisymmetric and non-axisymmetric longitudinal/torsional modes. Gazis's approach was called the normal mode expansion (NME) method. In addition, Gazis states numerical results on cutoff frequencies, the frequency vs. wavelength spectra, and compares his results with the shell theory solution. By applying Gazis's method, which is called normal mode expansion (NME), Rose obtained the wave structures of axisymmetric modes in hollow cylinders [2].

Ditri and Rose built upon Gazis's NME method to calculate the amplitude of any guided wave mode in a hollow cylinder [5]. They used excitation source loading to determine the amplitudes. Based on this research, Li and Rose [6] studied the energy distribution of axisymmetric and non-axisymmetric longitudinal modes. This facilitated the simulation of wave motion angular profiles generated by the partial loading of a hollow cylinder. According to the angular profiles, phased array focusing was achieved by applying time delays to N partially loaded excitation sources equally spaced around the circumference of a hollow cylinder. The input parameters of the guided wave phased array focusing technique are nonlinear functions of a focal distance. Unlike the bulk wave focusing techniques, it depends on the amplitude and phase of the angular profile for each excitation channel [7]. Li and Rose developed a deconvolution focusing algorithm using single excitation source angular profiles. Sun et al. developed the angular profile simulation and phased array focusing techniques for torsional waves in hollow cylinders [8-10]. Zhang and Rose stated that the wave structure of a wave mode group is determined not only by the frequency and pipe size but also by the excitation conditions [12].

1.3 Objectives

Because the guided wave focusing technique is successfully utilized to improve the pipe inspection results, it becomes important to study focusing potential as a guide for future industrial, military, or academic applications of this technique. In order to investigate the phased

array focusing potential in cylindrical structures, the study of guided wave velocities and particle motions must be carried out first. One may calculate the velocities and displacements of guided waves in isotropic elastic straight pipes by implementing the normal mode expansion (NME) method. Based on these data, the focusing results can be calculated.

In this study, theoretical simulations and experiments will be conducted to study the influence of the variations of the excitation frequencies and transducer sizes for phased array focusing and natural focusing. Variation of circumferential locations and frequencies of a partial loading can improve the natural focusing results. For a pipe with non-axisymmetric geometries (such as defects and elbows) or material inhomogeneities (such as anisotropic welds), some numerical approaches have to be used instead of the analytical calculations to simulate the guided wave behaviors. These efforts will show the possibility of achieving the phased array focusing or natural focusing in a particular pipeline.

SECTION 2

PIPE INSPECTION POTENTIAL WITH THE FOCUSING TECHNIQUES

2.1 Defect Detection with the Phased Array Focusing Technique

2.1.1 The Phased Array Focusing Algorithm

The analytical calculations for the velocities and displacement distributions of guided waves in an isotropic elastic tubular medium are presented in Appendix A. Some important concepts, such as axisymmetric mode, flexural mode, wave group, dispersion curves, and angular profiles, are also defined in Appendix A. By assuming that the frequency, the incident angle, and the circumferential loading length of all elements are identical in a phased array, the phased array focusing technique for guided wave propagation in hollow cylinders was achieved by Li and Rose [17]. In their research, an ultrasonic transducer array with N (N>1) individual excitation sources was used to focus the ultrasonic energy at a particular position by applying the pre-determined time delays and amplitude controls for the input signals. The excitation sources are equally spaced around the circumference of the pipe. Based on the simulations of the angular profiles of a transducer (Appendix A), the time delays and amplitudes of the input signals for phased array focusing can be calculated by a deconvolution process.

Supposing that every excitation channel of the array has the same loading conditions as shown in Equation (A.24) or Equation (A.26), the focused angular profile function G can be obtained from the angular profile function H at a distance z_0 as follows:

$$G = A \otimes H \tag{2.1}$$

where the unknown discrete complex function A works as a weight function; $\otimes$ is the convolution operator; H indicates the discrete angular profile of a single excitation channel. The simulation process of H was illustrated in the Appendix A [6, 8].

When the guided waves are focused at the 0° circumferential location of the hollow cylinder at a distance z_0, the focused angular profile function G becomes a pulse function in the circumferential direction. In another words, if using the element i (i = 1,2,3,…,N) of G to represent the excitation channel i, the discrete function is described as:

$$G = [G_i]_{N\times 1}; \quad G_i = \begin{cases} 1, & (i = 1) \\ 0, & (1 < i < N) \end{cases}. \tag{2.2}$$

The algorithm for the discrete weight function A is expressed as:

$$A = G \otimes^{-1} H = FFT^{-1}(G / H) \tag{2.3}$$

where $\otimes^{-1}$ and FFT^{-1} denote deconvolution and the inverse fast Fourier transform operator, respectively.

In order to achieve focusing, the discrete function A can be used to determine the input coefficients to superimpose ultrasonic energy from all of the single excitation sources. The phase delay and amplitude of the input signal for the excitation channel i is the phase ϕ_i and the amplitude L_i of the corresponding weight function A_i. Consequently, the input time delay for channel i is:

$$\Delta t_i = -\phi_i / 2\pi f \tag{2.4}$$

The phase delays ϕ_i in a sample problem presented in Figure 2-1 are calculated by employing the deconvolution algorithm for 4-channel phased array focusing. The circumferential loading length is 90°. A 60kHz L(m,1) wave group (The mathematical definition of a wave group can be found in Appendix A) was used to focus at 0° at z_0 = 366" in a 16" Schedule 30 steel pipe. Figure 2-1 illustrates the correlation of the phase of the L(m,1) single excitation source profile with the corresponding deconvolution phase delays for focusing. It shows that the phase delay for each channel matches the single-element profile phase at the same circumferential angle. Therefore, by applying the time delays to the input signals, one can align the phase of the guided wave group and achieve focusing. The amplitude controls for the input signals are utilized to reduce the side lobes of the focal energy beam.

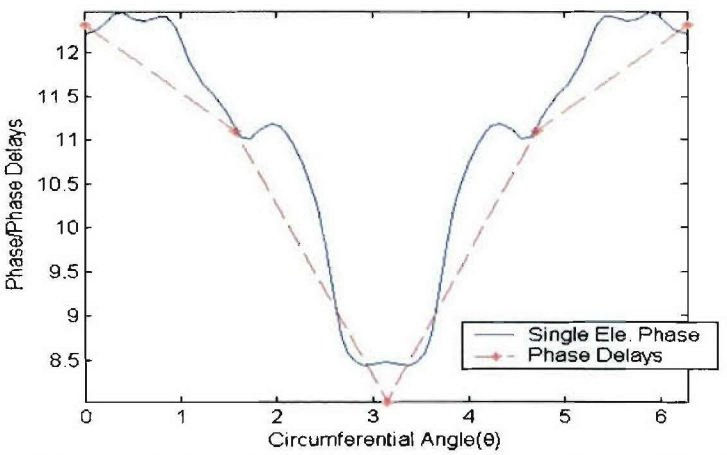

Figure 2-1. Phase delays and phase for a single channel angular profile of the L(m,1) wave modes propagation in 16" Schedule 30 steel pipe with 90° loading at 60kHz.

2.1.2 Spinning the Focal Spot

The focal spots of phased array focusing in hollow cylinders are based on the angular profile function G. Because the circumferential length of one excitation transducer in the phased array is usually not small enough to be neglected, one has to determine the center location of the focal spots within the circumferential loading area. If the circumferential loading length of one transducer is 2α and the center of the transducer is at the 0° (Figure A-4), a circumferential

location θ_1 $(-\alpha < \theta_1 < \alpha)$ can be selected as the center of the focal beam. The Equation (2.2) becomes:

$$G = [G_i]_{N\times 1}; \quad G_i = \begin{cases} 1, & (\theta = \theta_1) \\ 0, & (\theta \neq \theta_1) \end{cases} \tag{2.5}$$

Substituting Equation (2.5) into Equation (2.3) yields the input coefficients for focusing at θ_1. Figure 2-2 shows sample results of focusing the 35kHz T(m,1) group in a 16" schedule 80 steel pipe at z = 180" at 0°, 10°, 20°, 30°, and 40°. The circumferential loading length of each transducer is 90°. When the energy is focused at the center of the transducer (0°), the side lobes of the focal beam become smallest; when the energy is focused at or close to the edge of the transducer, the side lobes are almost as large as the main focal lobe. In other words, it is difficult to concentrate the ultrasonic guided wave energy at a circumferential location aligned with the edge of a transducer in the phased array. Therefore, the pipe inspection by applying the phased array focusing technique tends to choose the circumferential location of the center of a transducer for the focal spot. In order to achieve the best focusing results, if it is required to sweep a focal spot, we usually change the locations of the transducers instead of moving the focal spot within the circumferential length of a transducer.

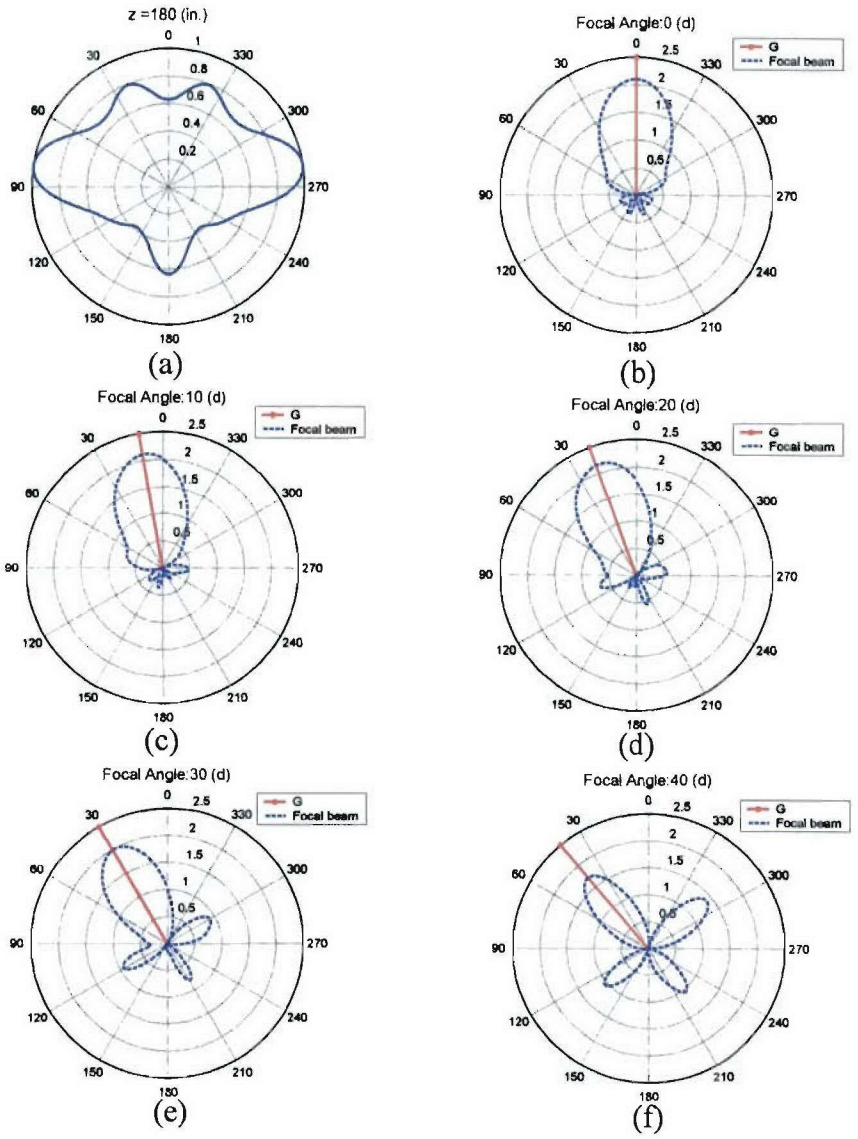

Figure 2-2. Sample angular profiles of the L(m,2) mode group in a 4" schedule 40 steel pipe at frequency f = 100kHz, 200kHz, 300kHz, and 400kHz.

By sweeping the focal spot in the circumferential direction, one can utilize the phased array technique to locate individual defects.

2.2 Defect Detection by Frequency and Angle Tuning

2.2.1 Axisymmetric Excitations with Frequency Tuning

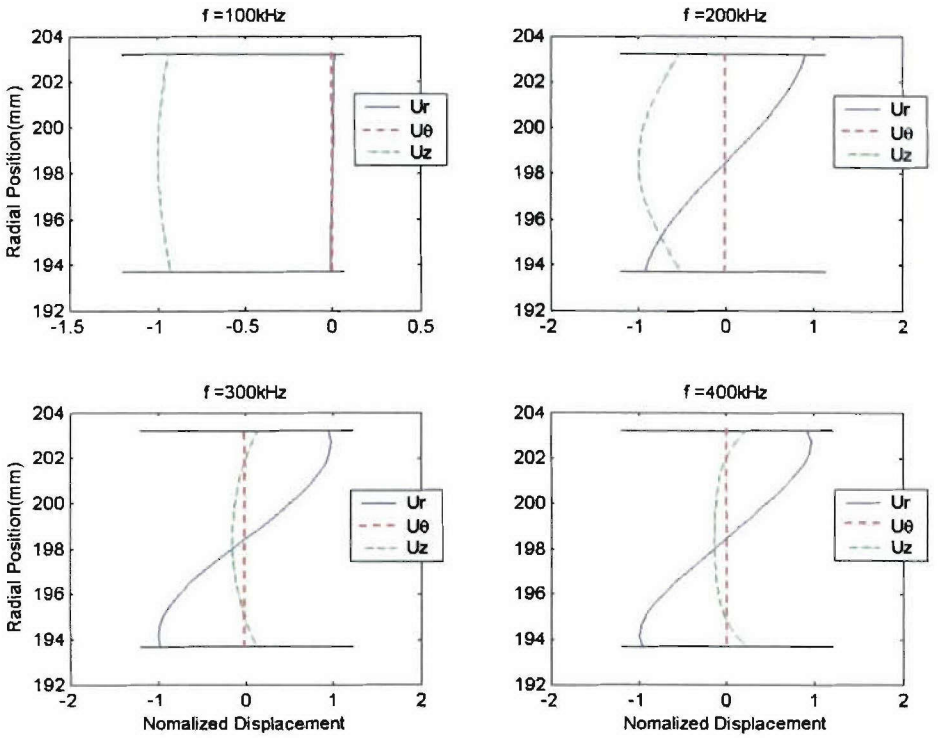

Figure 2-3. Wave structures of the L(m,2) mode group in a 16" schedule 30 steel pipe at the frequency = 100kHz, 200kHz, 300kHz, and 400kHz.

As shown in Appendix A, wave structures of a guided wave (group) are highly frequency-dependent. Figure 2-3 shows the wave structures of the L(m,2) group in a 16" schedule 30 steel pipe. It can be seen that not only the displacement distribution in the radial direction but also the dominant particle motion direction change with the variation of frequencies. Guided waves with different dominant particle motion directions are sensitive to defects with different shapes. In addition, reflection signals become more significant when more ultrasonic energy is impinged onto a defect. Tuning frequency may make the energy increase at the radial position of a defect. Hence, the frequency tuning technique can be utilized to improve the guided wave sensitivity of particular defects.

2.2.2 Natural Focusing with Frequency and Angle Tuning

Sometimes a partial circumferential excitation is the only way a pipe could be loaded because of accessibility limitations. By applying a partially loaded excitation on a hollow cylinder, the energy of ultrasonic guided waves may be naturally focused at some distances (Figure 2-4). This phenomenon is called "natural focusing". Because it might be possible to develop natural focal spots within the inspection range at a particular frequency, there will not be enough energy distributed at the other positions. For example, the 60kHz T(m,1) group excited by a transducer with a 90° circumferential length is focused on the top of an 8" schedule 40 pipe at an axial distance of z = 702" , although most energy is distributed at the bottom at z =342". Consequently, some defects at these positions become non-detectable. On the other hand, since the ultrasonic energy is enhanced at the focal spots, the natural focusing can be utilized to

improve the guided wave pipe inspection results, especially if the natural focal spots can be moved throughout the structures.

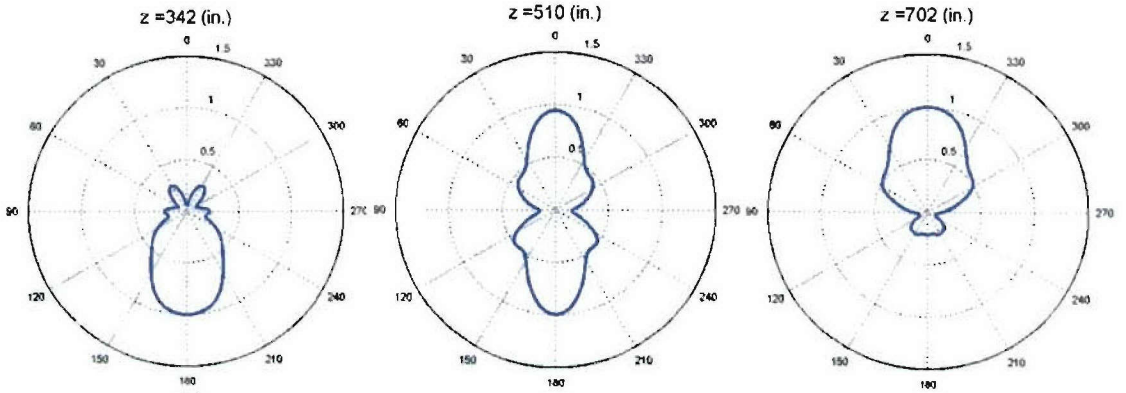

Figure 2-4. Sample angular profiles of the 60kHz T(m,1) mode group in a 8" schedule 40 steel pipe with a 90° circumferential excitation length. The transducer is located at $\theta = 0°$ and z = 0 (in.). The angular profiles are at the axial distances: (a) 342", (b) 510", and (c) 702".

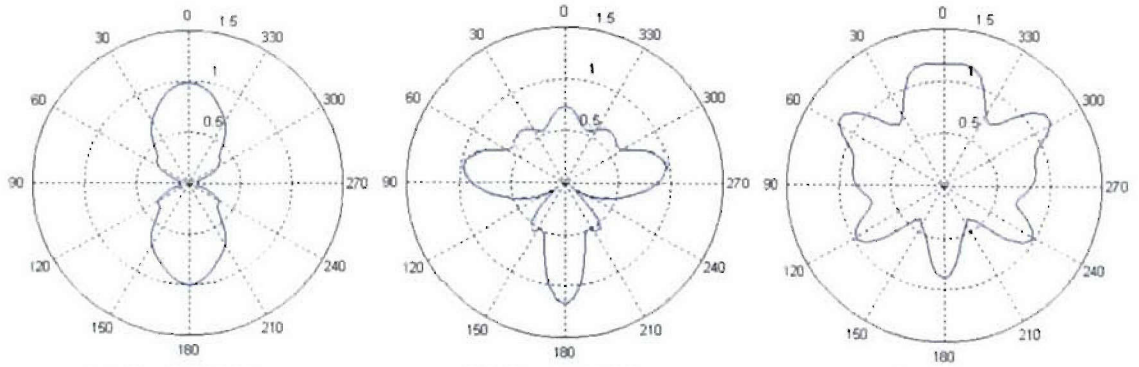

Figure 2-5. Sample angular profiles of the L(m,1) mode group in a 4" schedule 40 steel pipe at z=180" with a 90° circumferential excitation length. The transducer is located at $\theta = 0°$ and z = 0 (in.). The frequency f is (a) 200kHz; (b) 400kHz; (c) 600kHz.

The location of the natural focal points, however, changes with not only the axial distance but also with the frequency. As shown in Figure 2-5, the shape of an angular profile is highly dependent on frequency. Therefore, in order to detect all of the defects in a hollow cylinder by utilizing natural focusing, a frequency tuning technique is required to change the positions of the focal spots. Most sections of a pipe can be thoroughly inspected by tuning frequency over some appropriate range. For the other sections, one has to change the location of the excitation source in order to scan the entire tube. The partially loaded excitations with variations of the frequencies and excitation locations are called "frequency and angle tuning (FAT)" technique.

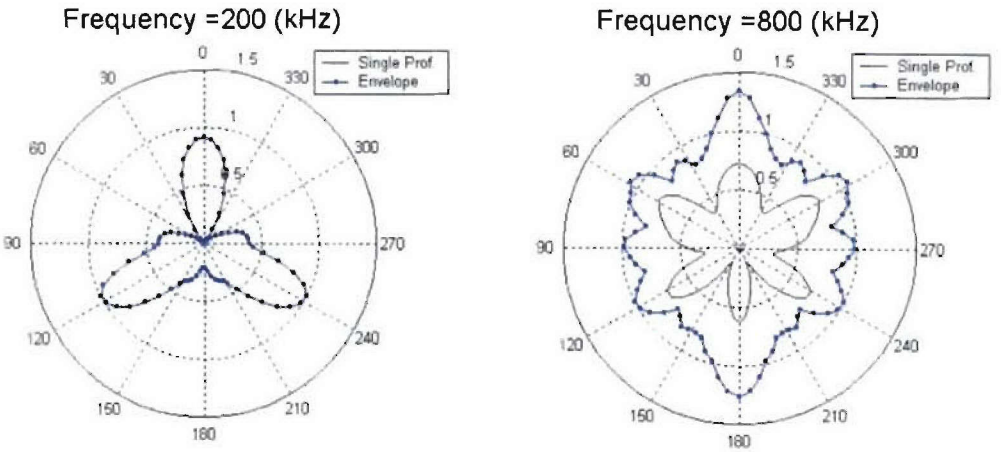

(a) (b)

Figure 2-6. Sample angular profiles and their envelope of the T(m,1) mode group in a 4" schedule 40 steel pipe at z=180" with a 90° excitation angle. The frequency f is (a) 200kHz; (b) 800kHz.

The angular profiles of a mode group can be calculated by using the algorithm shown in Appendix A. By recording the envelope of the angular profile variations of the T(m,1) group in a 4" schedule 40 steel pipe at z = 180", one can see that there is enough energy at all of the circumferential locations by sweeping frequency over the range: 200kHz-800kHz (Figure 2-6). The black lines indicate the angular profiles at the particular frequency and the blue lines denote the envelope of all the angular profiles at the former frequencies. Figure 2-6(b) illustrates the angular profile at 800kHz and the overall of the angular profile envelope over the frequency range: 200kHz-800kHz.

Theoretical simulations show that the angular profile verifications are highly dependent on the differences between the velocities of the wave modes in a group. If all of the flexural wave velocities are close to the axisymmetric wave velocity, the angular profiles change slowly with the axial distances and the frequencies. A large pipe with a thin wall has more similar wave velocities in a group than a pipe with a smaller diameter and a relatively thick wall. Generally, the wall thickness to diameter ratio of an industry pipeline decreases with an increase in diameter. In another words, the angular profiles in hollow cylinders with small diameters usually vary faster than in large pipes over the same frequency range. Therefore, a sufficient frequency range for natural focusing inspections in pipelines varies for different pipe.

In addition, the flexural mode velocities tend to converge to the axisymmetric mode velocity at a high frequency. Hence, high frequency natural focusing inspection needs a larger frequency tuning range than the lower frequencies. Figure 2-7 illustrates the angular profiles and their envelopes of the T(m,1) and L(m,1) groups propagating in a 16" schedule 30 steel pipe. Although the pipe is larger than the 4" pipe in Figure 2-6, the adequate inspection frequency range becomes smaller for these low frequency natural focusing detections. Nevertheless, because the inspection sensitivity for defects in a cylindrical shell essentially depends on the

wave lengths of the guided waves, high frequency and short wave lengths are necessary for detecting small defects.

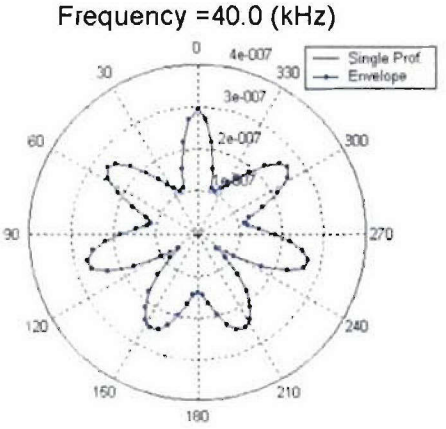

(a) L(m,1) group at 40kHz

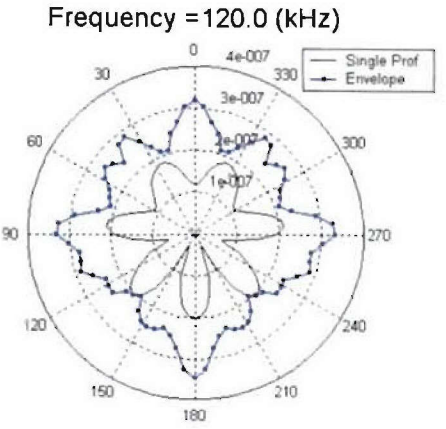

(b) L(m,1) group at 120kHz

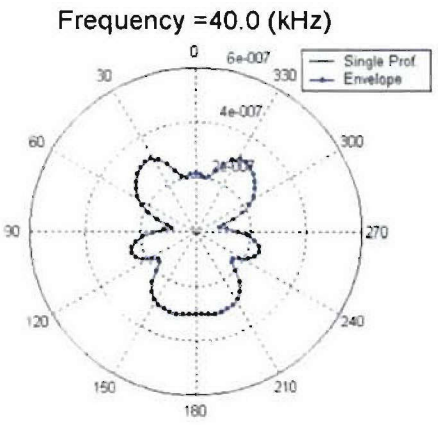

(c) T(m,1) group at 40kHz

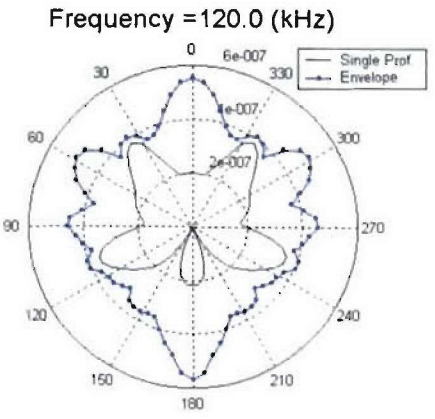

(d) T(m,1) group at 120kHz

Figure 2-7. Sample angular profiles and their envelopes of the L(m,1) and T(m,1) mode groups in a 16" schedule 30 steel pipe at z=18' with a 90° excitation angle. The angular profiles and their envelopes involve: (a) 40kHz L(m,1) group, (b) 120kHz L(m,1) group, (c) 40kHz T(m,1) group, (b)120kHz T(m,1) group.

Theoretical simulations and experimental results shows that the entire cross sectional area of a hollow cylinder may not be inspected thoroughly at all axial distances by applying natural focusing with frequency tuning. Combined with circumferential loading length variations, however, frequency tuning might be possible to get complete inspection coverage at more axial distances. Nevertheless, for the axial distances that are not far from the transducer position, the energy beams are always aligned with the transducer. The angular profile variations in a 2" schedule 40 steel pipe were investigated, as can be seen in Figure 2-8. By applying a -22.5° ~ 22.5° partial loaded excitation at z = 0", the maximum amplitudes of the angular profile envelopes were measured in different circumferential areas: channel 1 (0°~45°), channel 2 (45°~90°), channel 3 (90°~135°), and channel 4 (135°~180°). Figure 2-8(b) shows the maximum

values of the displacements at each channel at the axial distance range: 8"~122". The excitation frequency range of the partially loaded guided wave generator is from 200kHz to 800kHz. For a small axial distance z, the angular profiles are constantly focused at the channel 1, which is at the same circumferential position as the transducer.

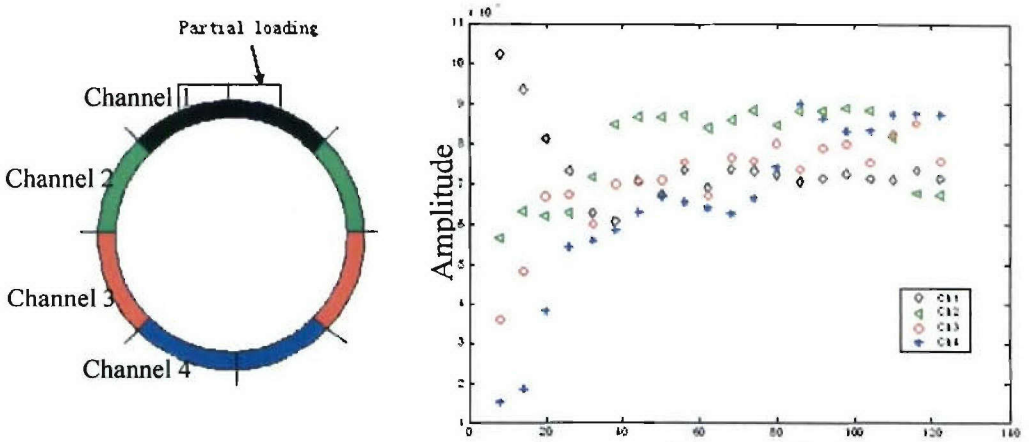

(a) (b)

Figure 2-8. Sample maximum displacement amplitudes in different circumferential areas of a 2" schedule 40 steel pipe over a frequency tuning range from 200kHz to 800kHz at z=8"~ 122". The circumferential excitation length is 45°.

The simulation result in Figure 2-8 shows that the guided wave energy is concentrated on the same circumferential location as the excitation transducer within 20" from the wave generator. For a larger pipe, this natural focal zone will increase. Therefore, tuning the circumferential loading location is required to inspect the entire cross sectional area of a pipe by utilizing the natural focusing phenomenon. Because natural focusing with the FAT technique can increase the energy impinging onto any defect in a cylindrical shell, the guided wave inspection sensitivity and accuracy for pipelines are consequently improved.

In Figures 2-9 and 2-10, a series of angular profiles of the L(m,1) group are calculated at two different axial distances where some defects were located at 106 inches from the sensor and some at 82 inches, respectively. In Figures 2-9 and 2-10, it can be seen that the angular profile of a single transducer changes drastically with frequency variations. The lower right hand corners of Figures 2-9 and 2-10 illustrate the so-called FAT envelope effect. This includes both frequency and circumferential loading angle tuning. The overall envelopes are pretty complete from 0° to 360° in scanning the cross sectional area at the particular axial locations. Angle tuning includes data of exciting the L(m,1) group at every 45° around the circumference for either the 45° or 90° circumferential loading length. Comparing the angular profiles in Figure 2-9 (a) to the ones in Figure 2-9 (b), one can see that the circumferential loading length significantly affects the angular profiles. In some cases, although the FAT technique provides a complete coverage of ultrasonic energy throughout the pipe, some circumferential loading lengths might be better than others.

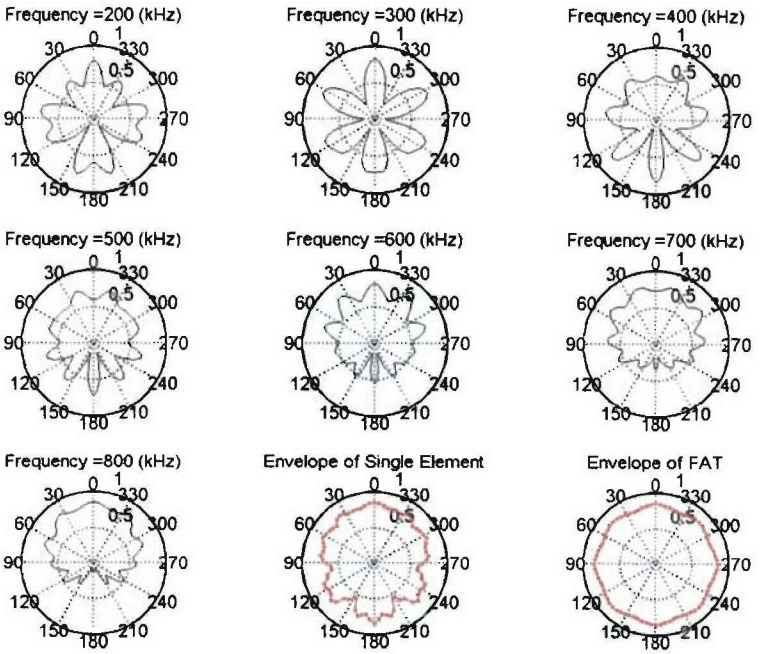

(a) Circumferential excitation angle: 45°

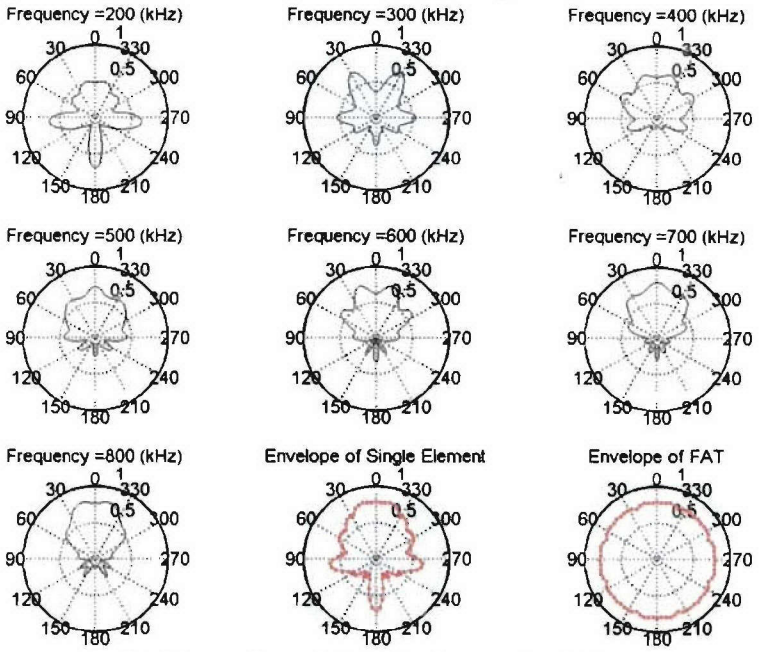

(b) Circumferential excitation angle: 90°

Figure 2-9. At an axial distance z=82", the L(m,1) mode group angular profiles and their envelope over the frequency range 200kHz~800kHz in a 4" schedule 40 steel pipe with circumferential excitation angle (a) 45° and (b) 90°. The transducer is located at $\theta = 0°$ and z = 0 (in.).

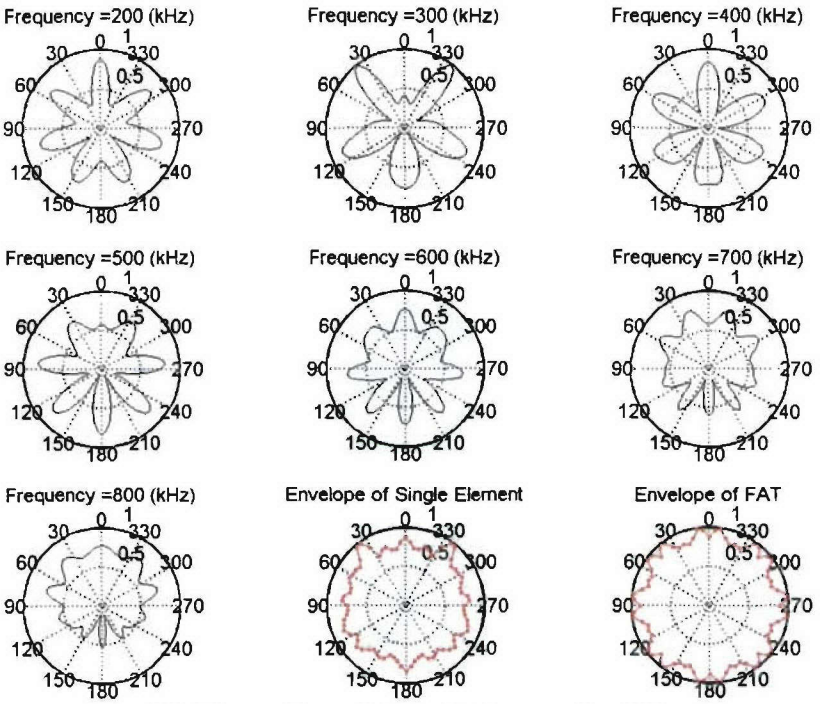

(a) Circumferential excitation angle: 45°

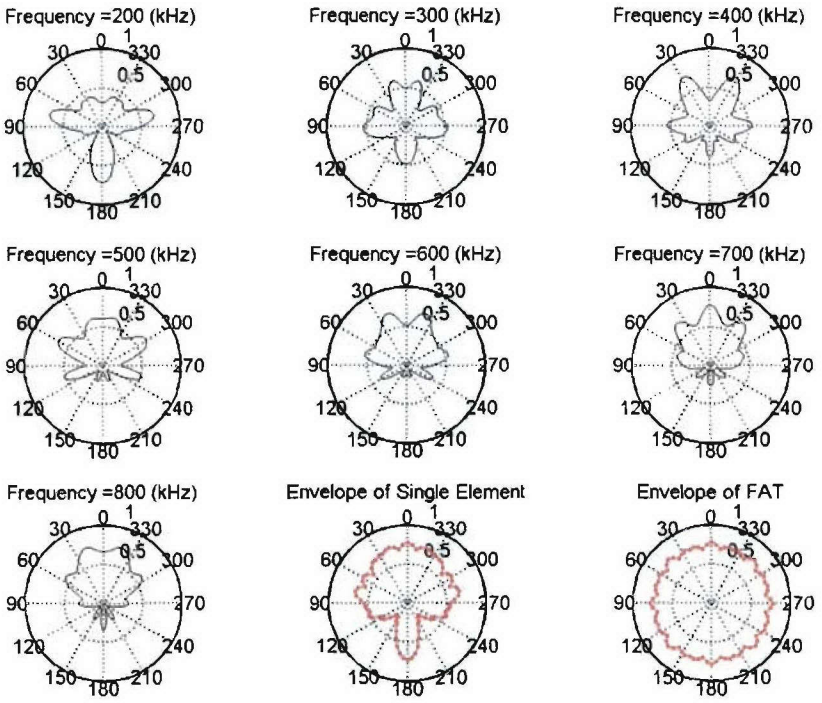

(b) Circumferential excitation angle: 90°

Figure 2-10. At an axial distance at z=106", the L(m,1) mode group angular profiles and their envelope over the frequency range 200kHz~800kHz in a 4" schedule 40 steel pipe with circumferential excitation angle (a) 45° and (b) 90°. The transducer is located at $\theta = 0°$ and z = 0 (in.).

2.2.3 Experimental Results

Experiments were conducted to carry out guided wave natural focusing with FAT in 4" schedule 40 and 8" schedule 40 steel pipes. The experimental setups are shown in Figure 2-11. The ultrasonic guided wave generation system includes a commercial ultrasonic signal generation system, Matec®, and a high frequency piezoelectric transducer array. According to Snell's Law, the incident angle of each transducer is set to excite the L(m,1) mode group.

The 4" pipe illustrated in Figure 2-12 contains two defects: a 0.22% CSA 5-Hole cluster at z=82" and a 1.01% CSA round bottom hole at z=106" from the transducer array. Partial loading with the FAT technique was applied at both pipe ends A and B. The axisymmetric excitation with frequency tuning over the same frequency range was also studied for comparison purposes. The envelopes of the ultrasonic signals generated by the axisymmetric excitations and partial loadings over the frequency range [200kHz, 800kHz] are shown in Figure 2-13. The axisymmetric inspection result in Figure 2-13(a) with excitation from the pipe end A does not locate the two defects with much certainty. Results are poor, when exciting at the pipe end B. The round bottom hole (RBH) echo appears quite clearly, although the echo from the five-hole cluster is still buried in the noise. If utilizing the so called FAT technique for 90° circumferential excitation, one can detect the round bottom hole from the both pipe ends and see the RBH and the five-hole cluster when loading at the pipe end A, as shown in Figure 2-13c and 2-13d. By changing the circumferential excitation length to 45°, one achieves the best inspection results with visible echoes from the two defects by excitation at either pipe end.

Similarly, the FAT technique was used to test another pipe, as shown in Figure 2-14. In this case, the FAT technique along with the axisymmetric inspection technique is illustrated in Figure 2-15. The FAT technique also achieved better inspection results than the axisymmetric excitation. For this pipe with the same size as the pipe in Figure 2-12, the FAT inspections with 90° partial loading obtained better results than the ones with 45° partial loading. In other words, the best circumferential loading length depends on not only the pipe size but also on the locations and geometries of the defects.

These experiments proved that natural focusing with FAT can improve the guided wave inspection results for defects in tubular structures.

Figure 2-11. Experimental equipment, which includes the specially developed Matec® ultrasonic A-scan 8-channel control system and a high frequency phased array on a 4" schedule 40 pipe for 200kHz~800kHz frequency tuning inspection.

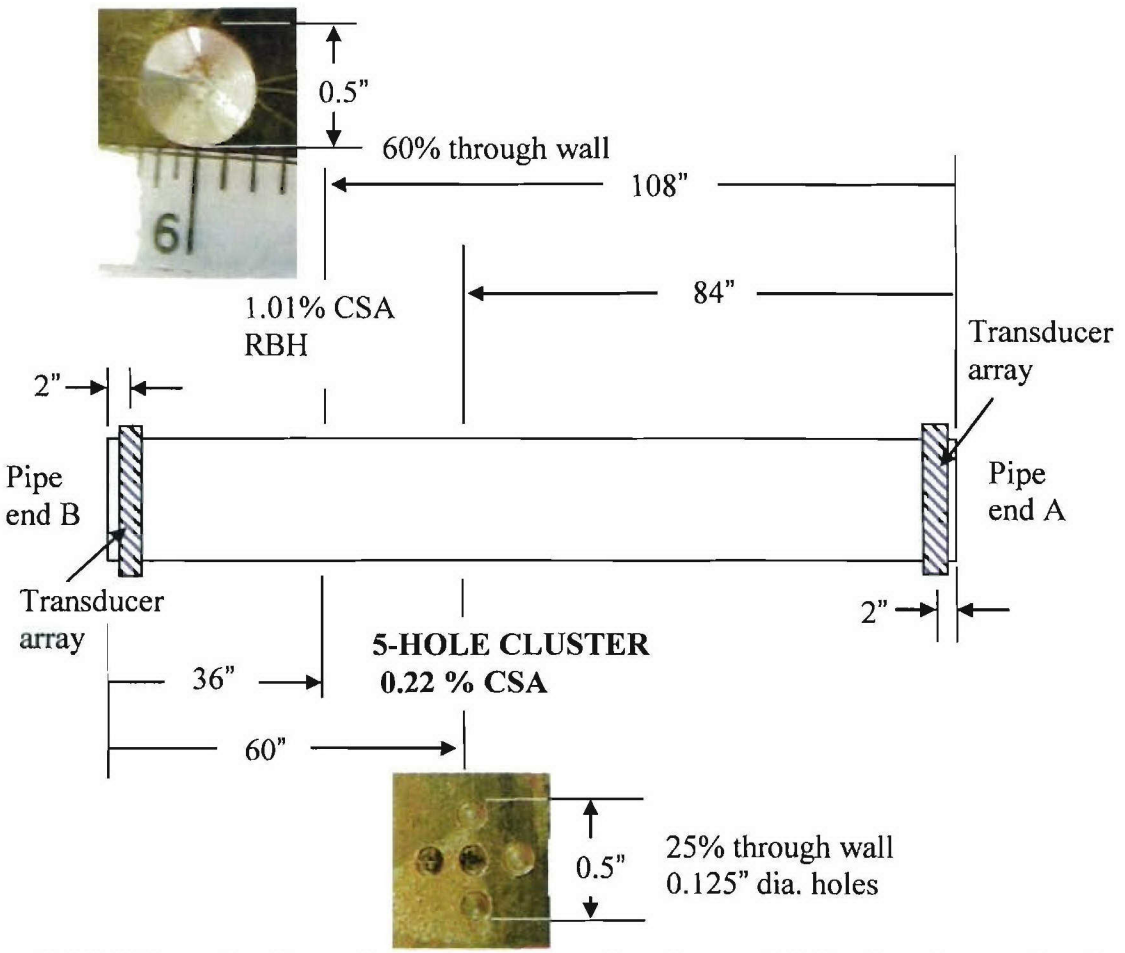

Figure 2-12. Schematic ultrasonic transducer array locations and defect locations at the pipe #1, which is a 4" schedule 40 steel pipe.

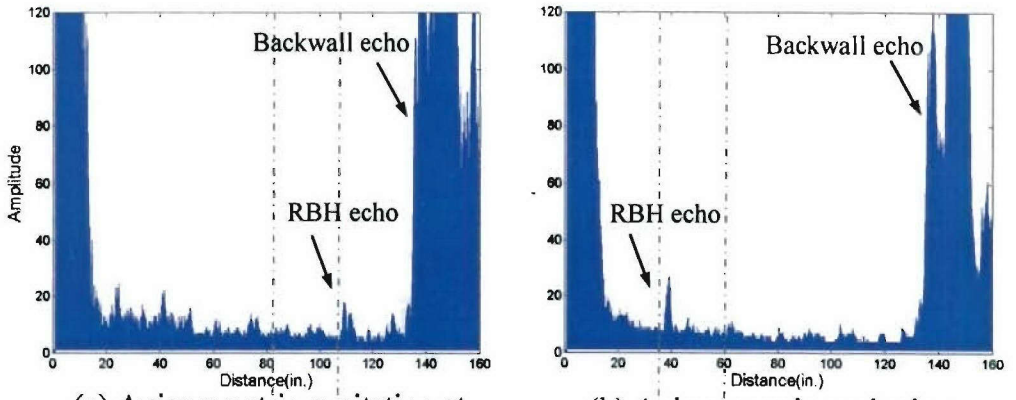

(a) Axisymmetric excitation at the pipe end A

(b) Axisymmetric excitation at the pipe end B

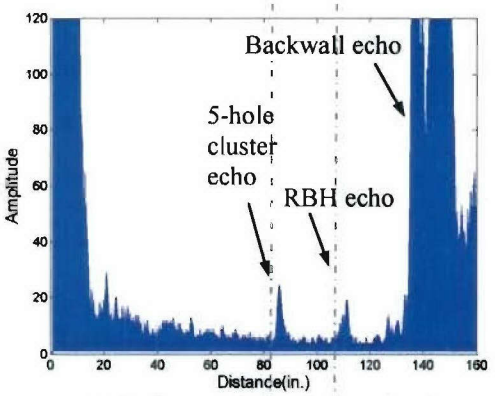

(c) 90° circumferential excitation angle at the pipe end A

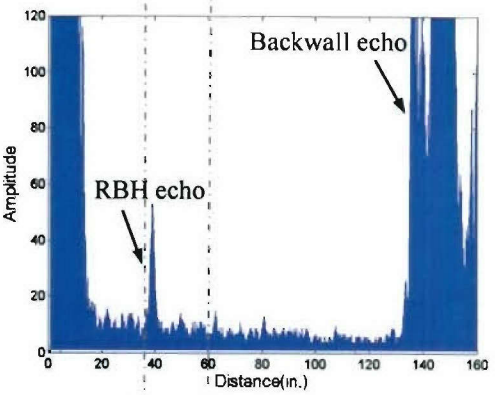

(d) 90° circumferential excitation angle at the pipe end B

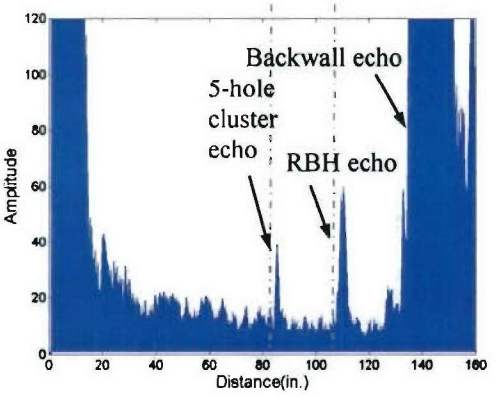

(e) 45° circumferential excitation angle at the pipe end A

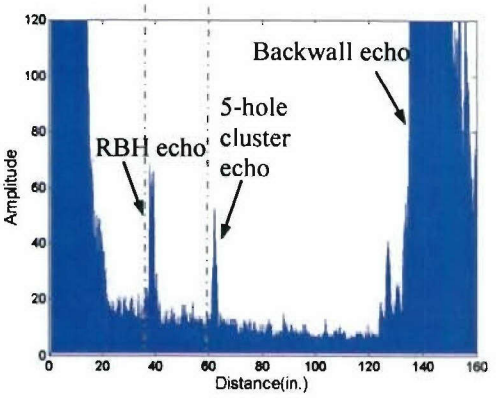

(f) 45° circumferential excitation angle at the pipe end B

Figure 2-13. Maximum amplitudes of the axisymmetric and FAT natural focusing inspection results pipe #1. The defects include a 0.22% CSA 5-Hole cluster at 84" and a 1.01% CSA RBH at 108" from the pipe end A.

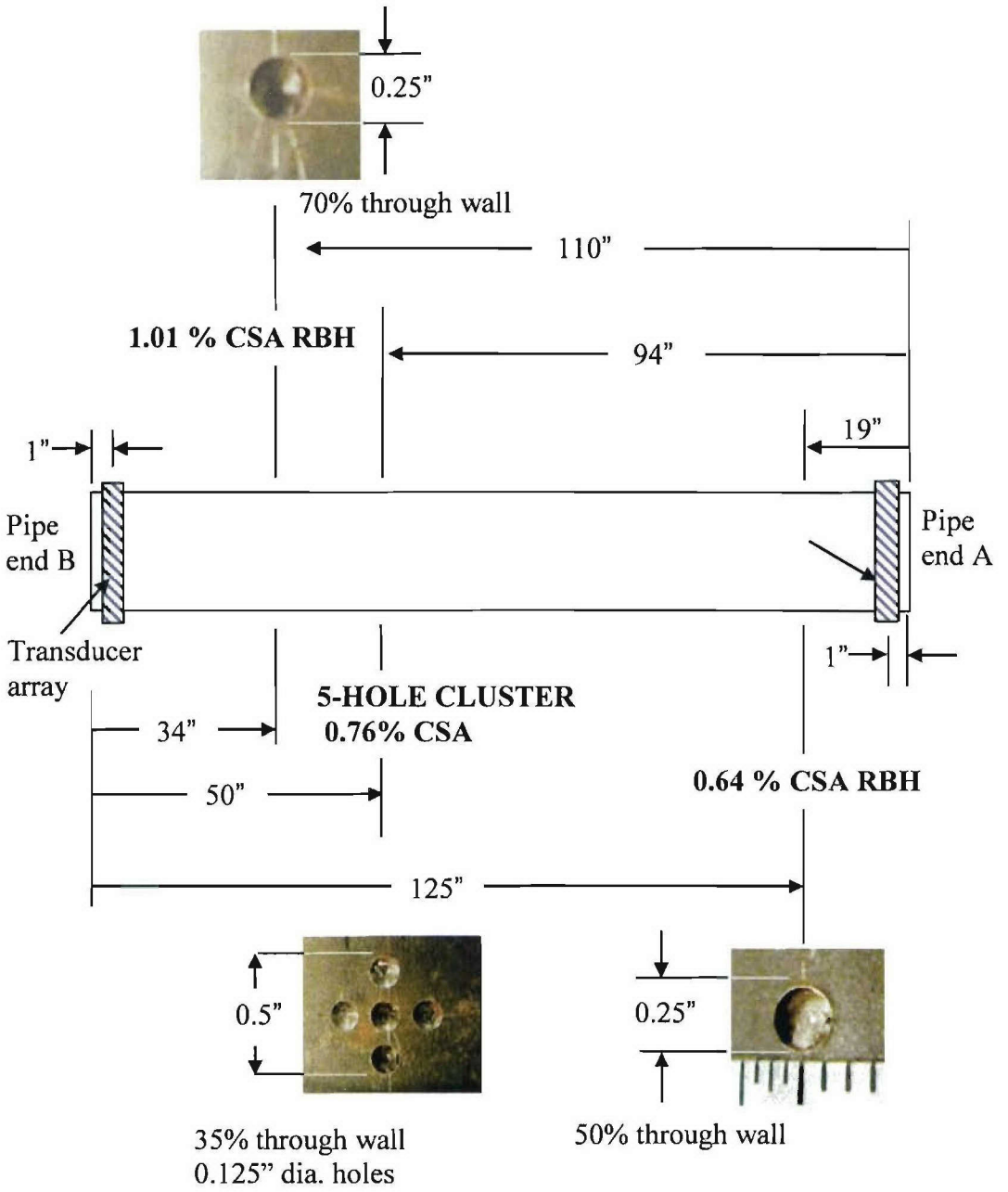

Figure 2-14. Schematic of ultrasonic transducer array locations and defect locations at the pipe #2, which is a 4" schedule 40 steel pipe.

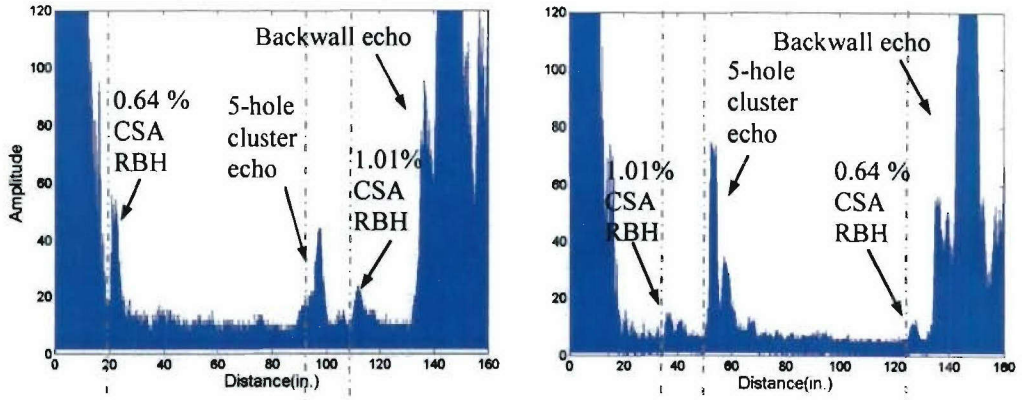

(a) Axisymmetric excitation at the pipe end A

(b) Axisymmetric excitation at the pipe end B

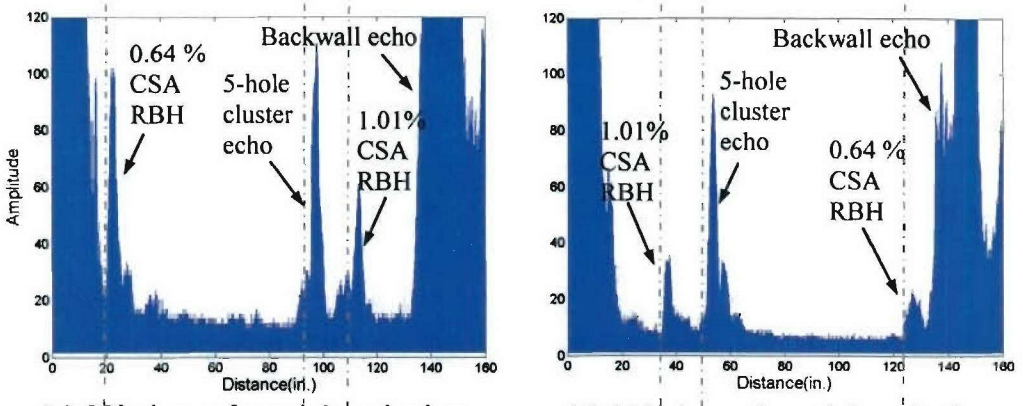

(c) 90° circumferential excitation angle at the pipe end A

(d) 90° circumferential excitation angle at the pipe end B

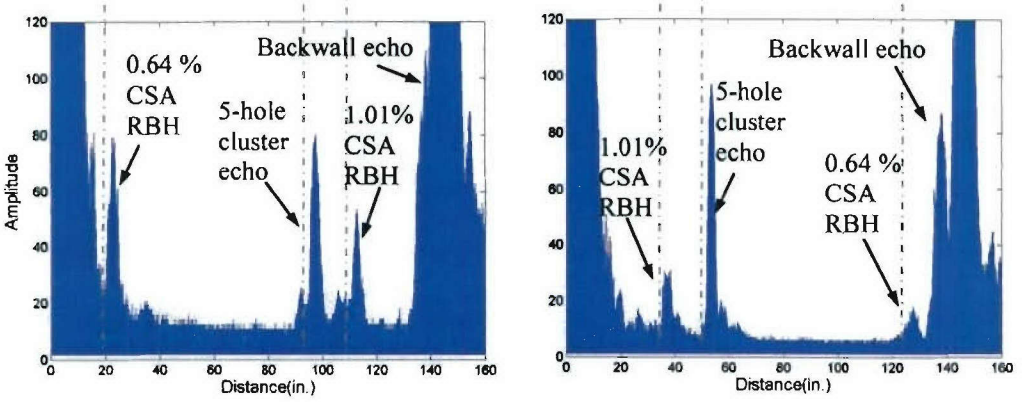

(e) 45° circumferential excitation angle at the pipe end A

(f) 45° circumferential excitation angle at the pipe end B

Figure 2-15. Maximum amplitudes of the axisymmetric and FAT natural focusing inspection results for pipe #2. The defects include a 0.64% CSA RBH, a 0.76% CSA 5-Hole cluster at 94" and a 1.01% CSA RBH at 110" from the pipe end A.

2.3 Summary

We first reviewed the phased array focusing algorithm for guided waves in hollow cylinders. An algorithm of focal spot variation was developed to concentrate guided wave energy at different circumferential locations. By changing the input time delays and amplitude controls of the phased array, the focal spots can be moved in both the circumferential direction and axial directions. In addition, the phased array focal spots also change with a variation of the transducer locations. Comparing the amplitudes of the defect signals when focusing at different circumferential angles at the axial location of a defect, one can determine the approximate circumferential location of a defect. Experiments were conducted to verify the focusing algorithm and the possibility of locating defects.

The natural focusing inspection technique is also investigated. If partially excited guided waves are naturally focused at some particular positions with a single excitation frequency, some areas in a hollow cylinder may not have enough energy for defect inspection, which is calling for techniques to alter the natural focal point locations. In order to solve this problem and to benefit from the energy improvement by utilizing the natural focusing technique, more excitation frequencies and circumferential loading locations are required. Since the angular profiles from a partial excitation source highly depends on the frequency and loading angle, the natural focal spots vary when applying the so-called FAT technique. Both theoretical simulations and experimental results indicate that an entire hollow cylinder can be sufficiently inspected by implementing the guided wave natural focusing inspection with the FAT technique.

Besides the phased array focusing and the natural focusing techniques, one can take advantage of frequency tuning with an axisymmetric excitation which can also be used to enhance the ultrasonic energy impinging onto a defect, hence improving the axisymmetric inspection results.

SECTION 3

SOURCE INFLUENCE FOR GUIDED WAVES IN CYLINDRICAL SHELLS

3.1 Source Influence for Guided Wave Generation

Phased array focusing in a cylindrical structure is achieved by applying excitation time delays to a multi-channel signal generation system. Natural focusing with the FAT technique includes use of partial loading and frequency and loading angle tuning. For both focusing techniques, the angular profiles generated by a single excitation source determine focusing potential. These angular profiles are dependent upon excitation source influences. Before studying the excitation source influence for focusing potential, we have to investigate the source influence for guided wave generation in a hollow cylinder.

The theoretical simulations of ultrasonic guided wave propagation in tubular structures by using the normal mode expansion method are shown in Appendix A. Based on Equations (A.25) and (A.27), some parameters affecting the generation of guided waves are listed in Table **3-1**:

Table **3-1**: Parameters affecting guided wave generation in an elastic isotropic hollow cylinder

Parameters	Influence for the guided waves
Pipe diameter and thickness	Wave velocities
Material properties of pipe	Wave velocities
Motion direction of the excitation	Type of guided waves
Frequency and frequency bandwidth	Frequency and frequency bandwidth
Phase velocity and velocity bandwidth	Phase velocity and velocity bandwidth
Sizes of the excitation sources	Amplitude of every wave mode

Since the properties of a pipe are unchangeable, the excitation sources become the only factor that can be used to influence the guided wave distribution and focusing potential. The most important parameters of the excitation sources involve: 1) excitation type, which includes the

particle motion direction of the excited wave modes and the frequency bandwidth, the velocity bandwidth and the wave number of the incident waves; 2) the circumferential and axial size of the excitation source.

Two typical ultrasonic transducers illustrated in Figure 3-1 include: (a) a piezoelectric transducer on an angle beam wedge, and (b) an Electromagnetic Acoustic Transducer (EMAT). According to Snell's Law, the angle beam wedge excites guided waves with a constant phase velocity when utilizing a predetermined incident angle. In Figure 3-2, the red circle on the red horizontal dashed line indicates the excitation zones of an angle beam transducer with a fixed incident angle. The EMAT/comb type transducer generates guided waves with a constant wavelength equal to the spacing of the elements. The excitation zones are on the blue dashed line in Figure 3-2. The slope of the excitation line is determined by the wavelength. Besides the angle beam transducers which only excite a constant velocity, there is a normal beam transducer with a normal incidence onto the specimen. Since the normal beam can excite all of the possible wave modes at a given frequency, it is usually used at a low frequency in which only a few mode groups exist.

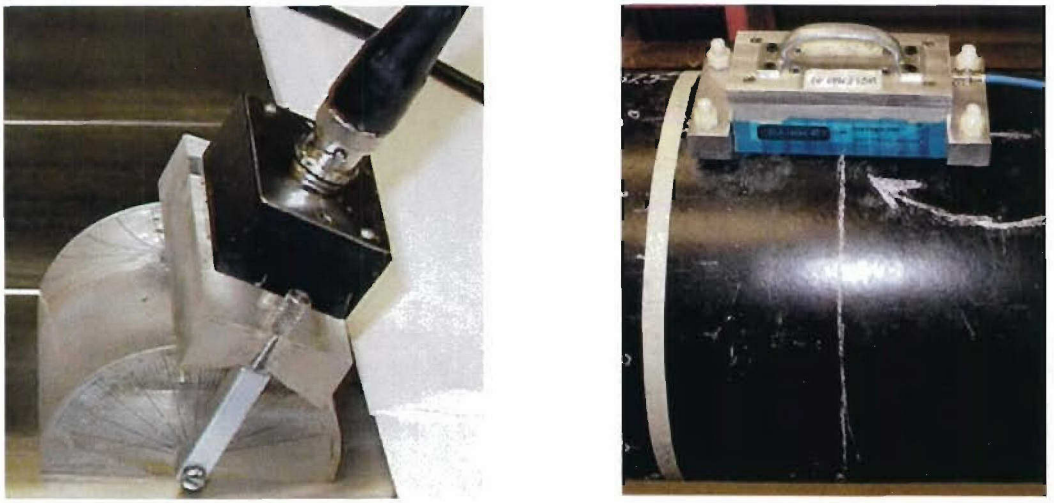

(a) Angle beam transducer (b) EMAT

Figure 3-1. Sample guided wave generators.

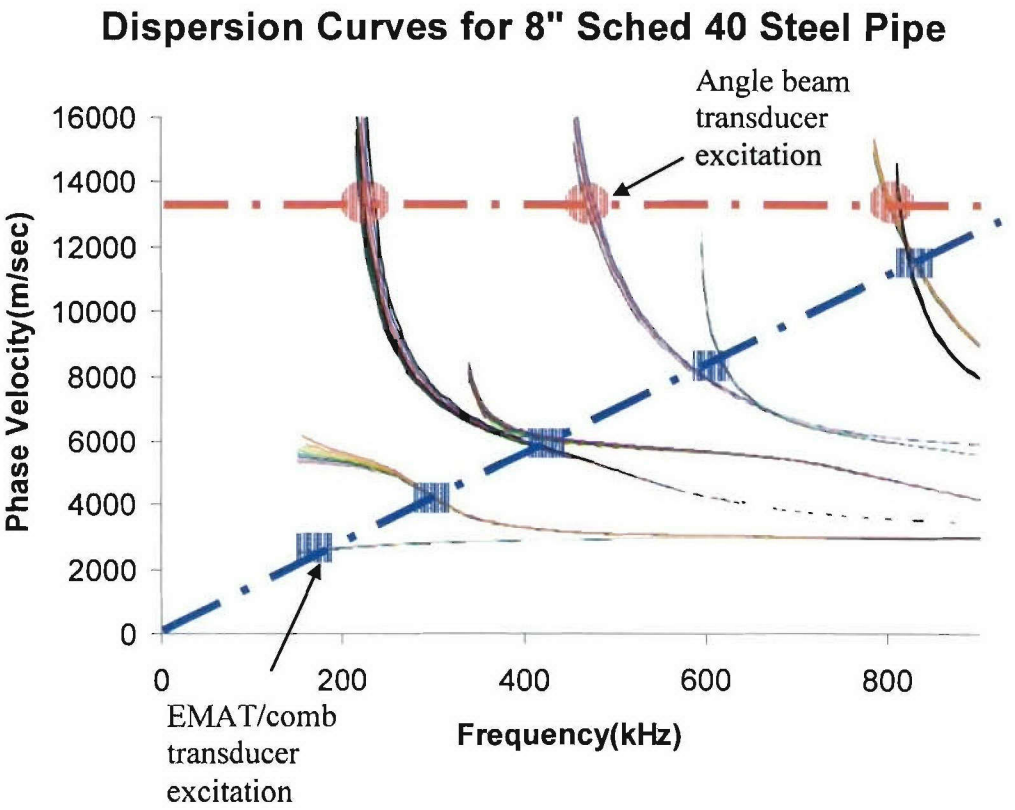

Figure 3-2. Sample excitation zones of an angle beam transducer and an EMAT/comb transducer on the longitudinal dispersion curves of an 8" schedule 40 steel pipe. The blue dashed line indicates the possible EMAT/comb transducer excitation line for a given element spacing; the red dashed line indicates the possible angle beam transducer excitation line for a particular incident angle.

Snell's Law for angle beam incidence is expressed as:

$$\frac{c_1}{c_2} = \frac{\sin\theta_1}{\sin\theta_2} \tag{3.1}$$

where the c_1 and c_2 denote the velocities of the incident wave and the refracted wave; θ_1 and θ_2 are the incident angle and the refracted angle.

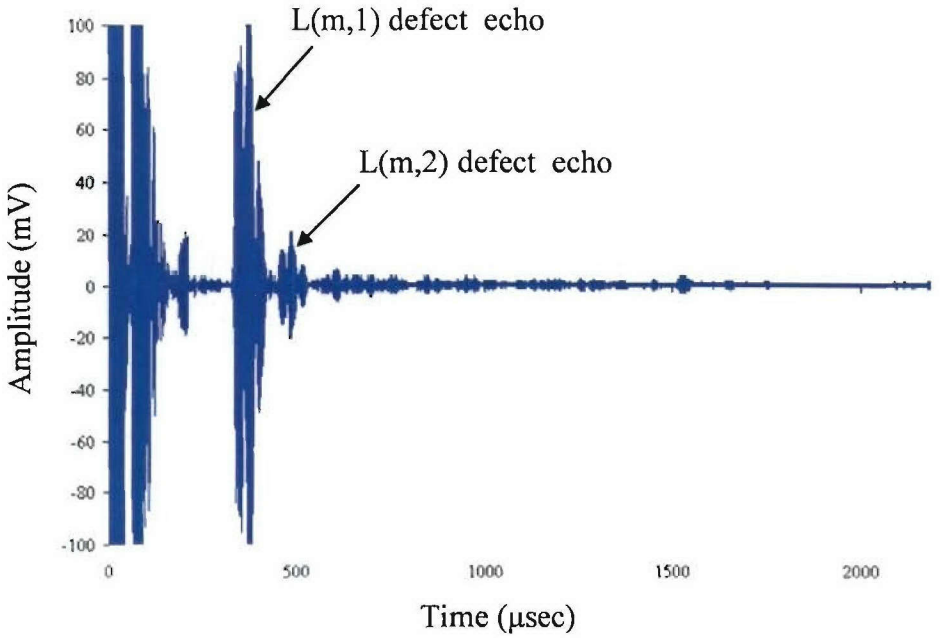

Figure 3-3. Sample wave form of 45° partially loaded 650kHz longitudinal guided waves in an 8" schedule 40 steel pipe.

Because the guided waves are usually not only generated at one frequency or at one phase velocity, the frequency bandwidth and the phase velocity bandwidth are important transducer parameters. All of the wave groups in the excited frequency band and phase velocity band may be generated. For example, using an angle beam transducer to excite a L(m,1) mode group at 650kHz in an 8" schedule 40 steel pipe should generate the L(m,2) group, since the phase velocities of these two groups are similar at 650kHz, as can be seen in Figure 3-2. The angle beam transducers shown in Figure 2-10 have an incident angle to produce the 650kHz L(0,1) mode in an 8" steel pipe. According to the wave form in Figure 3-3, both the L(m,1) and L(m,2) groups were generated by applying these angle beam transducers with a 45° circumferential length on the 8" schedule 40 steel pipe.

The possible wave type generated by a transducer depends on the particle motion direction. For instance, an EMAT that produces guided waves with shear particle motion cannot excite the L(m,1) mode group over the frequency range [20kHz, 800kHz], because the dominant particle motion of the L(m,1) modes is in the radial direction.

3.2 Source Influence for the Energy Distribution in Hollow Cylinders

Besides the properties of the incident wave, there are two source influence factors in Equations (A.25) and (A.27) that affect the amplitudes of the modes in a group (Figure A-4):
1) circumferential loading angle 2α
2) axial excitation length $2L$
Because the amplitude of each mode determines the overall energy distributions, especially the angular profiles in a hollow cylinder, the axial and circumferential sizes of the ultrasonic transducers are considered as the factors that decide the energy distributions in pipes.

When considering the excitation conditions in Equations (A.24) and (A.26), one can see that the loading functions are separated in the circumferential and axial direction. Generally, the circumferential loading distribution function $p_1(\theta)$ is a constant p_0 in the excitation area:

$$p_1(\theta) = \begin{cases} p_0, & -\alpha \le \theta \le \alpha \\ 0, & -\alpha > \theta, or \quad \theta > \alpha \end{cases} \tag{3.2}$$

Based on Equation (3.2) and Equation (A.25) and (A.27), the amplitude of the axisymmetric mode divided by the amplitude of a flexural mode contains the following part, which is decided by the function $p_1(\theta)$:

$$\frac{\int_{-\alpha}^{\alpha+2\pi} \Theta_r^m(m\theta) p_1(\theta) d\theta}{\int_{-\alpha}^{\alpha+2\pi} \Theta_r^0(0) p_1(\theta) d\theta} = \frac{\sin(m\alpha)}{m\alpha}, \text{ m} = 1, 2, 3, \ldots \tag{3.3}$$

The axial loading distribution function $p_2(z)$ depends on the incident wave properties. The normal beam excitations and the excitations with constant incident wave numbers, such as angle beam transducers and EMAT/comb transducers, have different $p_2(z)$ functions.

The function $p_2(z)$ for normal beam excitation is:

$$p_2(z) = \begin{cases} 1, & |z| \le L \\ 0, & |z| > L \end{cases} \tag{3.4}$$

Based on Equation (3.4) and Equation (A.25) and (A.27), the amplitude of the axisymmetric mode divided by the amplitude of a flexural mode in a same group contains the following part, which depends on the function $p_2(z)$:

$$\frac{\int_{-\infty}^{\infty} p_2(z) e^{ik^{mn} z} dz}{\int_{-\infty}^{\infty} p_2(z) e^{ik^{0n} z} dz} = \frac{k^{0n} \sin(k^{mn} L)}{k^{mn} \sin(k^{0n} L)}, \quad \text{m, n} = 1, 2, 3, \ldots \tag{3.5}$$

To generate a desired mode M(0,n) (M denotes L or T), the incident wave generated by an angle beam transducer or an EMAT must contain the wave number k^{0n}. Therefore, the function $p_2(z)$ for this type of excitation is:

$$p_2(z) = \begin{cases} e^{-ik^{0n} z}, & |z| \le L \\ 0, & otherwise \end{cases} \tag{3.6}$$

which leads to:

$$\frac{\int_{-\infty}^{\infty} p_2(z)e^{ik^{mn}z}dz}{\int_{-\infty}^{\infty} p_2(z)e^{ik^{0n}z}dz} = \frac{\sin[(k^{mn}-k^{0n})L]}{(k^{mn}-k^{0n})L}, \quad \text{m, n} = 1, 2, 3, \ldots \tag{3.7}$$

Comparing Equation (3.5) and (3.7), it can be concluded that the results for these equations are close when the axial transducer length L and the difference between the two wave numbers $|k^{mn}-k^{0n}|$ are small enough. However, if the axial length of the transducer is large or the dispersion curves diverge, these two equations have totally different solutions. For example, if one lets the frequency = 150 kHz, m = 9, n = 2 and L = 30 mm for guided wave generation in a 4" schedule 40 steel pipe with the dispersion curves shown in Figure A-2, the result for Equation (3.5) is -3.5421 and for Equation (3.7) is -0.1089. The results are totally different, because the phase velocities of the L(m,2) modes diverge from each other at this frequency.

Assuming $\left|k^{mn}-k^{0n}\right| \to \infty$ or $\left|k^{mn}-k^{0n}\right| > 0$ and $L \to \infty$ makes the value of Equation (3.7) become zero, although $\frac{k^{0n}\sin(k^{mn}L)}{k^{mn}\sin(k^{0n}L)}$ does not converge to zero. In other words, an axially infinitely long transducer will only generate an axisymmetric wave even with a partial loading. Because the focusing phenomenon is caused by flexural modes, it is impossible to achieve focusing by using an infinitely long excitation source. Similarly, the focusing technique will not work when the wave numbers of the flexural modes have large differences from the axisymmetric wave velocity in the same group. For instance, most flexural modes in the L(m,2) group are cut-off at 150kHz in Figure A-2; $\left|k^{mn}-k^{0n}\right|$ becomes infinite for the modes and focusing cannot be accomplished for the L(m,2) group at this frequency.

In conclusion, the "converging" dispersion curves at a particular frequency and a limited axial length of the excitation source are required to perform focusing in a tubular structure. Since the size of an ultrasonic transducer is limited, usually, at least six flexural modes existing in a group is necessary to achieve reasonably good focusing results.

Equation (3.3) shows that the amplitude of a flexural mode depends highly on the circumferential length of the excitation source. When α increases, the energy in the flexural mode with a large order number m will decrease. If $2\alpha = 2\pi$, it becomes an axisymmetric excitation and only the axisymmetric mode (m=0) will exist. Therefore, an excitation transducer with a small circumferential length excites more flexural modes. A larger number of flexural modes usually make the energy distribution change more sharply in the circumferential direction. Therefore, the angular profiles in a cylindrical shell are sensitive to the circumferential loading length.

3.3 Source Influence for Phased Array Focusing Potential

3.3.1 Theoretical Evaluation of Phased Array Focusing Potential

For clarity, phased array focusing potential is defined as the ability to generate a focused angular profile at a predetermined circumferential and axial location by using a multi-channel ultrasonic phased array. According to Li and Rose, the focusing results are determined by the angular profiles of a single excitation channel [7].

Let us consider the focusing potential of the guided waves generated by an N-channel ($N \geq 1$) guided wave generator system. The circumferential loading length of each excitation element is equal to $2\alpha = 360° / N$. The axial length of the excitation transducers is $2L$. The focused profiles can be calculated using Equations (2.3). All the channel inputs identical ultrasonic waves with a same input wave number k^{0n}, which is the wave number of the axisymmetric wave in the nth wave group.

Since small values of $\left|k^{mn} - k^{0n}\right|$ for most flexural modes in a group are required to accomplish focusing, Equation (3.5) and (3.7) will converge to 1 when the axial transducer length $2L$ is also small. The analytical simulations show that if the axial length of the excitation source is only several inches long, the axial transducer length $2L$ will not affect the angular profiles very much. Therefore, because the axial lengths of transducers are usually less than one foot, only the circumferential loading angle 2α should be considered as an important parameter for deciding focusing potential in hollow cylinders. Contour plots will be illustrated to show how the circumferential loading length influences the focusing potential.

In order to quantify focusing potential, the focusing criteria in a hollow cylinder are defined in Table **3-2**:

Table **3-2**: Focusing potential criteria

Focusing potential	*Criteria*
Bad	Focal region of the angular profile has less than 1.6dB improvement, or the most energy is distributed in out of the focal area;
Normal	Focal region of the angular profile has 1.6dB ~ 5dB improvement, or 25% ~ 45% of the energy is distributed out of the focal area;
Good	Focused region of the angular profile more than 5dB improvement, and most energy is focused;
Naturally Focused	Angular profile of a single excitation source is naturally focused. The phased array focusing results are almost the same as the natural focusing results.

Based on the criteria shown in Table **3-2**, the contour plots of circumferential loading length versus focusing potential in an elastic isotropic hollow cylinder can be accomplished by comparing the focal angular profiles to the axisymmetric energy distributions.

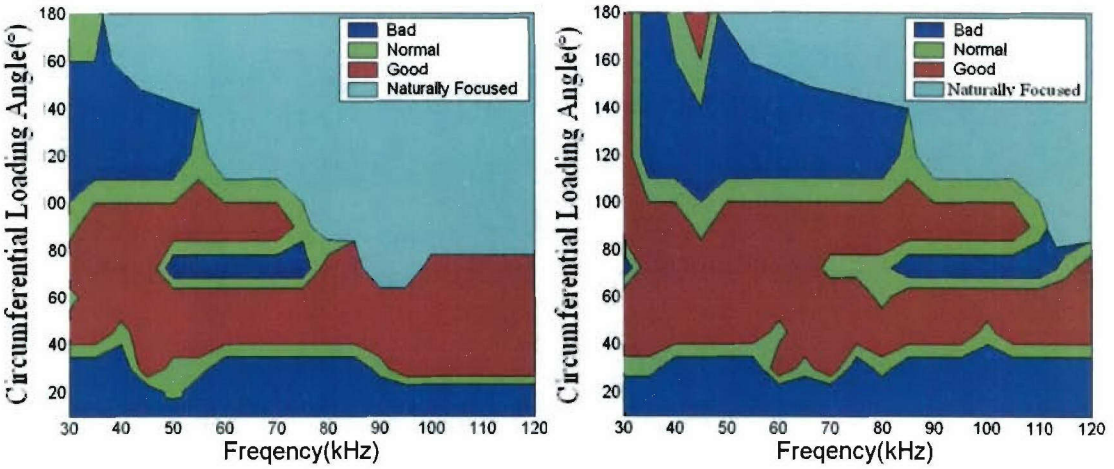

(a) at z = 240" (b) at z = 360"

Figure 3-4. Contour plots of focusing potential for the T(m,1) mode group at (a) z=240"and (b) z=360" in 16" schedule 30 steel pipe with circumferential excitation length from 10° to 180° over the frequency range: 30kHz~120kHz.

The sample contour plots of focusing potential at a high frequency range are presented in Figure 3-5 for the L(m,1) group in a 4" schedule 40 steel pipe. The 45° excitation length leads to best focusing potential. One can see that a high frequency range, larger pipe size, and smaller axial distance will cause the "naturally focused" area to extend in the contour plots.

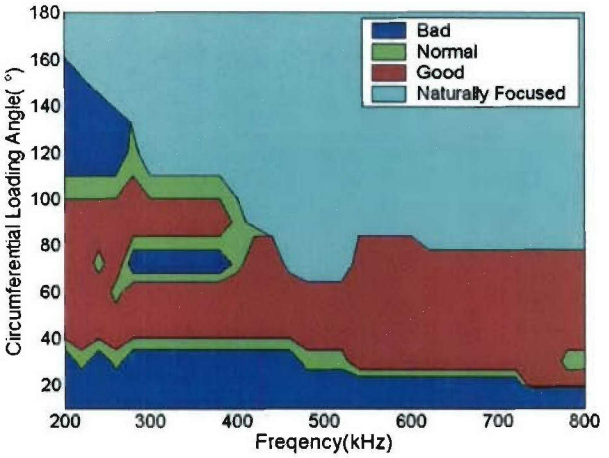

Figure 3-5. Focusing Potential for the L(m,1) mode group at z=110" in 4" schedule 40 steel pipe with circumferential excitation length from 10° to 180° over the frequency range: 200kHz~800kHz.

3.3.2 Experiment Verification

An experiment was carried out to achieve phased array focusing in a 4" schedule 40 steel pipe shown in Figure 2-13. According to the focusing potential chart in Figure 3-5, the 8-channel commercial Matec® system has "good" focusing potential at z=110" over the frequency range: 200kHz~800kHz. Although the phased array focusing at a high frequency requires more accurate time delay controls and better transducer alignment, we successfully focused the L(m,1) guided

wave group at the defect position and improved the detection results by about 6dB. See also Figure 3-6 where a frequency range from 200 to 800 kHz was considered.

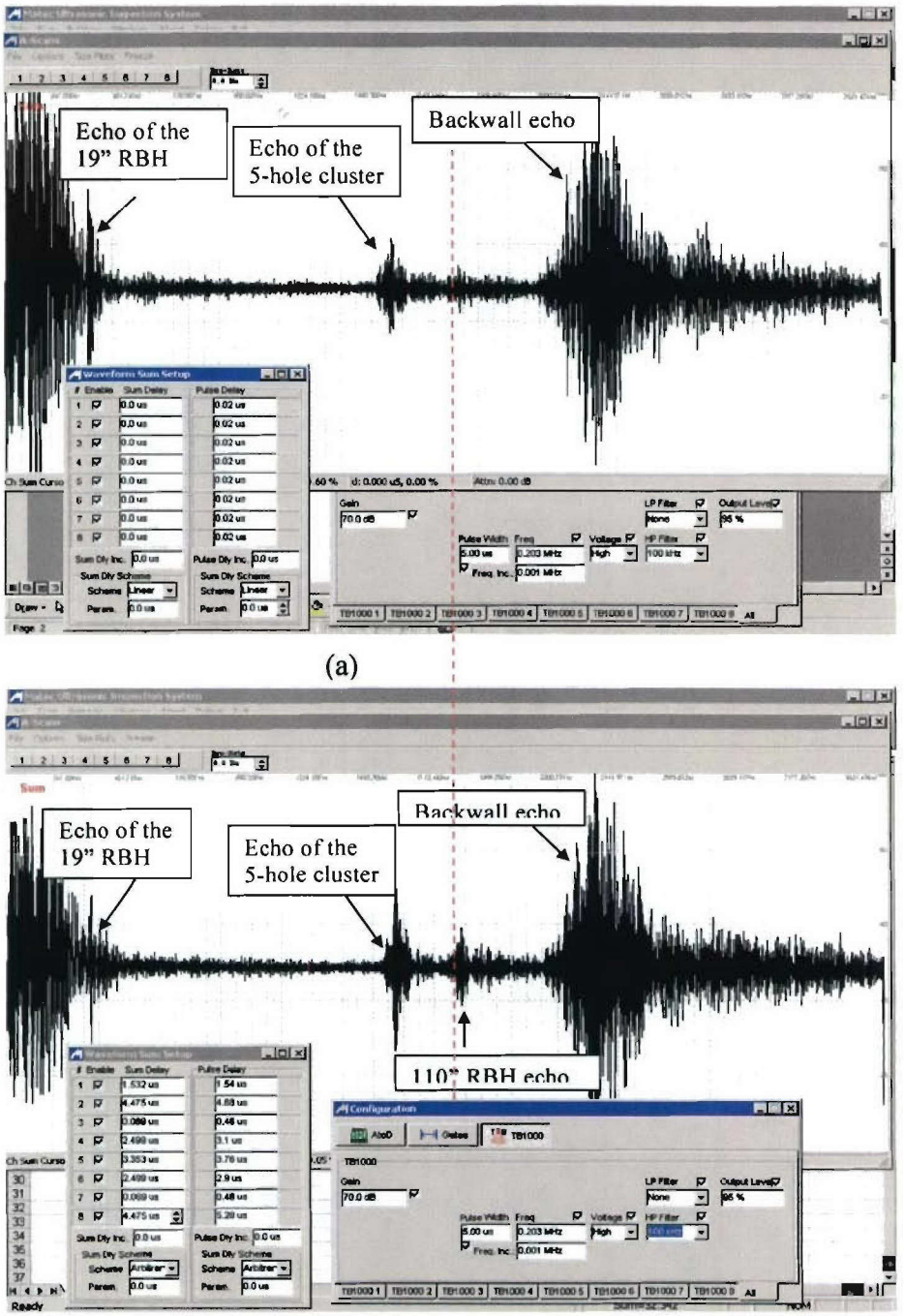

Figure 3-6. Ultrasonic signals by applying (a) axisymmetric excitation and (b) time delays to focus at a round-bottom hole at z=110". The echo from the 110" RBH is clearly shown when utilizing the phased array technique. Also the echo from a 5-hole cluster at z=94" is increased compared to the axisymmetric excitation, since the time delays also enhanced the energy at this defect position.

The experimental results of phased array focusing in hollow cylinders match the theoretical predictions quite well. Therefore, the contour charts of guided wave focusing potential in a tubular structure can be used to choose appropriate inspection parameters, such as loading length, frequency, wave type, and wave group.

3.4 Summary

Source influence for the focusing potential of guided waves in tubular structures was investigated. An angle beam transducer or an EMAT/comb type transducer can be used to select a particular wave mode group. In order to achieve focusing, the excitation source should have a finite axial length. A frequency at "converging" regions of the dispersion curves of a mode group is required to implement focusing. At this frequency region, a small axial excitation length rarely affects the angular profiles and focusing potential. Hence, the contour charts of focusing potential influenced by the circumferential excitation lengths were demonstrated. According to these contour plots, a large circumferential loading length may have good natural focusing potential and a tiny circumferential loading length may not lead to focusing at all. It is important to choose an appropriate excitation length and frequency to focus guided waves in a particular cylindrical shell. Finally, experiments were conducted to verify the analytical evaluations of the source influence theory. The focusing experiments had the same results as the theoretical predictions.

SECTION 4

CONCLUDING REMARKS

4.1 Summary and Concluding Remarks

Ultrasonic guided wave inspection is one of the most important non-destructive evaluation methods for pipeline safety. The sensitivity and accuracy of the guided wave pipeline inspection can be improved by utilizing focusing techniques, which most often increases the ultrasonic energy impinging onto the defects. Three typical focusing techniques were used in this research. These focusing approaches include the axisymmetric excitation with frequency tuning, the natural focusing with the FAT technique, and the phased array focusing. The axisymmetric excitation with frequency tuning can only change the wave structures of the guided waves; the FAT technique and the phased array focusing can alter both the wave structures and angular profiles. A brief comparison of the three focusing techniques is summarized in Table 4-1.

Table **4-1**: Focusing System Evaluation Features

Focusing Technique	Frequency Tuning	Natural Focusing	Phased Array Focusing
Defect detection sensitivity	good	very good	excellent
Possible inspection distance	long	longer	longest
Ability to determine circumferential location	poor	poor	excellent
Ability to determine circumferential length	poor	poor	excellent
Sufficient frequency band of transducer	broad band	broad band	either narrow or broad band
Types of wave modes	any	flexural modes needed	flexural modes needed
Axial length of transducer	any	finite length	finite length
Circumferential loading length	around the circumference	partial loading	phased array of partially loaded transducers
Inspection cost	reasonable	cheapest	expensive
Real time Inspection?	yes	no	yes

Because guided wave focusing techniques are not always achievable, it is important to investigate the guided wave focusing potential for pipe inspections. For a particular hollow cylinder, the guided wave focusing potential is determined by the excitation conditions, such as incident wave mode, excitation frequency and transducer size, and the geometry/material properties of the tubular waveguide.

There are many possible torsional and longitudinal groups of guided waves in a hollow cylinder. The particle motion direction, velocity and frequency of the incident wave will decide which

groups can be generated. The amplitude of each wave mode in this group depends upon the size of the excitation transducer. Usually, when the dispersion curves of a group are diverse at an excitation frequency or the axial length of the transducer is infinite, the amplitudes of the flexural modes become too small to achieve focusing. If the generated guided wave group is in a "converging" region of the dispersion curves and the axial length of the transducer is not very large (< 0.5m), only the circumferential length of the transducer will significantly affect the focusing potential in a cylindrical shell. Hence, contour plots of the circumferential loading length versus focusing potential were obtained to show the possibility of carrying out focusing in a particular hollow cylinder.

Besides the excitation conditions, the material and geometry inhomogeneities in the hollow cylinder may also leads to a failure to focus. In this research, the influences of anisotropic welds and some non-axisymmetric geometries (e.g. defects and elbows) for focusing potential were studied.

APPENDIX A

ANALYTICAL SIMULATIONS OF GUIDED WAVES IN HOLLOW CYLINDERS

A.1 Guided Wave Propagation in Hollow Cylinders

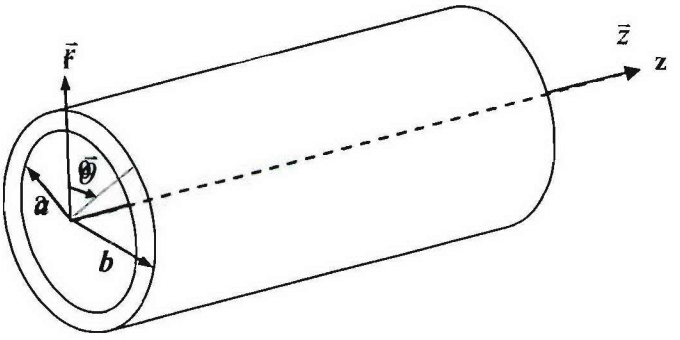

Figure A-1. Reference cylindrical coordinates

For an elastic isotropic hollow cylinder with traction-free boundary conditions on the inner and outer surfaces (Figure A-1), the wave propagation governing equation can be expressed as:

$$\mu\nabla^2\vec{U} + (\lambda+\mu)\nabla\nabla\cdot\vec{U} = \rho\left(\partial^2\vec{U}/\partial t^2\right) \tag{A.1}$$

where ρ presents the density, t is the time, and $\vec{U}$ indicates the displacement field, which is a function of the three cylindrical coordinates and time. The μ and λ are Lamé constants.

Let the displacement field $\vec{U}$ have a form as follows:

$$\vec{U} = \nabla\Phi + \nabla\times\vec{H} \tag{A.2}$$

where the Φ is a dilatational scalar potential and the $\vec{H}$ is an equivoluminal vector potential. An additional constraint is obtained from the gauge invariance analysis as Equation (A.3) [3]:

$$\nabla\cdot\vec{H} = 0 \tag{A.3}$$

Substituting Equation (A.2) into Equation (A.1) yields:

$$\nabla^2\Phi = \frac{1}{c_1}\frac{\partial^2\Phi}{\partial t^2} \tag{A.4}$$

$$\nabla^2\vec{H} = \frac{1}{c_2}\frac{\partial^2\vec{H}}{\partial t^2} \tag{A.5}$$

where c_1 is the longitudinal wave velocity and c_2 is the transverse wave velocity.
In cylindrical coordinates, the following are applicable:

$$\nabla^2\Phi = \frac{\partial^2\Phi}{\partial r^2} + \frac{1}{r}\frac{\partial\Phi}{\partial r} + \frac{1}{r^2}\frac{\partial^2\Phi}{\partial\theta^2} + \frac{\partial^2\Phi}{\partial z^2} \tag{A.6}$$

$$\vec{H} = H_r\vec{e}_r + H_\theta\vec{e}_\theta + H_z\vec{e}_z \tag{A.7}$$

$$\begin{aligned}\nabla^2\vec{H} &= \nabla^2\left(H_r\vec{e}_r + H_\theta\vec{e}_\theta + H_z\vec{e}_z\right)\\ &= (\nabla^2 H_r - \frac{1}{r^2}H_r - 2\frac{1}{r^2}\frac{\partial H_\theta}{\partial\theta})\vec{e}_r + (\nabla^2 H_\theta - \frac{1}{r^2}H_\theta\\ &\quad + 2\frac{1}{r^2}\frac{\partial H_r}{\partial\theta})\vec{e}_\theta + \nabla^2 H_z\vec{e}_z\end{aligned} \tag{A.8}$$

Assuming the following generalized solutions:

$$\begin{aligned}\Phi &= f(r)\Theta(m\theta)e^{i(kz-\omega t)}\\ H_r &= h_r(r)\Theta_r(m\theta)e^{i(kz-\omega t)}\\ H_\theta &= h_\theta(r)\Theta_\theta(m\theta)e^{i(kz-\omega t)}\\ H_z &= h_z(r)\Theta_z(m\theta)e^{i(kz-\omega t)}\end{aligned} \tag{A.9}$$

where k denotes the wave number; m is the circumferential order of a wave mode; the $\Theta(m\theta)$ and $\Theta_\xi(m\theta)$ (ξ = r, θ, z) are sinusoidal functions with respect to the wave type (longitudinal wave type or torsional wave type). The $f(r)$ and $h_\xi(r)$ (ξ = r, θ, z) are unknown coefficient functions. If only considering the axisymmetric wave modes, Equation (A.9) can be simplified [25] to be a 2-D problem, as:

$$\begin{aligned}\Phi &= f(r)e^{i(kz-\omega t)}\\ H_\theta &= h_\theta(r)e^{i(kz-\omega t)}\end{aligned} \tag{A.10}$$

Equation (A.10) shows the potential functions for the axisymmetric guided wave modes in tubular structures.

According to Zemanek [29], Meitzler [30], and Silk and Bainton [31], there are three mode types for time harmonic guided waves in hollow cylindrical media: 1) the axisymmetric longitudinal modes (L(0,n)), 2) axisymmetric torsional modes (T(0,n)), and 3) the flexural longitudinal and torsional modes (F_L(m,n) and F_T(m,n)). The longitudinal and torsional modes are axisymmetric. The flexural modes are non-axisymmetric and can appear in either longitudinal or torsional mode groups. For convenience, any mode in a longitudinal mode group will be renamed as L(m,n) and any mode in a torsional mode group as T(m,n). L(m,n) is an axisymmetric longitudinal mode when m = 0, else it is a non-axisymmetric flexural mode. T(m,n) is similar.

Let:

$$\alpha^2 = \omega^2/{c_1}^2 - k^2, \beta^2 = \omega^2/{c_2}^2 - k^2$$
$$\alpha_1 = |\alpha|, \quad \beta_1 = |\beta| \tag{A.11}$$

Substituting Equations (A.6)-(A.9) and (A.11) into Equations (A.4) and (A.5) gives:

$$\begin{aligned} f &= AZ_m(\alpha_1 r) + BW_m(\alpha_1 r) \\ h_3 &= h_z = A_3 Z_m(\beta_1 r) + B_3 W_m(\beta_1 r) \\ 2h_1 &= (h_r - h_\theta) = 2A_1 Z_{m+1}(\beta_1 r) + 2B_1 W_{m+1}(\beta_1 r) \\ 2h_2 &= (h_r + h_\theta) = 2A_2 Z_{m-1}(\beta_1 r) + 2B_2 W_{m-1}(\beta_1 r) \end{aligned} \tag{A.12}$$

where the Z_m and W_m are the mth order Bessel functions of different types, which are determined by the following definitions:

$$\begin{aligned} &c_1 k < \omega: \quad Z_m(\alpha_1 r), Z_m(\beta_1 r): J(\alpha r), J(\beta r); \quad W_m(\alpha_1 r), W_m(\beta_1 r): Y(\alpha r), Y(\beta r) \\ &c_2 k < \omega < c_1 k: \quad Z_m(\alpha_1 r), Z_m(\beta_1 r): I(\alpha_1 r), J(\beta r); \quad W_m(\alpha_1 r), W_m(\beta_1 r): K(\alpha_1 r), Y(\beta r) \\ &\omega < c_2 k: \quad Z_m(\alpha_1 r), Z_m(\beta_1 r): I(\alpha_1 r), I(\beta_1 r); \quad W_m(\alpha_1 r), W_m(\beta_1 r): K(\alpha_1 r), K(\beta_1 r). \end{aligned} \tag{A. 13}$$

Submitting Equation (A.12) into the gauge invariance Equation (A.3) gives:

$$\frac{1}{r}(h_1 + h_2 + rh_1' + rh_2' + mh_2 - mh_1 + ikrh_3) = 0 \tag{A.14}$$

Substituting Equation (A.6)-(A.9) and (A.12) into Equation (A.2) yields the displacement field. The displacement field for the longitudinal wave is:

$$\begin{aligned} U_r &= [f' + (m/r)h_3 + ikh_1 - ikh_2]\cos(m\theta)e^{i(kz-\omega t)} \\ U_\theta &= \left[-(m/r)f + ik(h_1 + h_2) - h_3'\right]\sin(m\theta)e^{i(kz-\omega t)} \\ U_z &= \left[-ikf + h_2' - h_1' - (m+1)(h_1/r) - (m-1)(h_2/r)\right] \\ &\quad \cos(m\theta)e^{i(kz-\omega t)} \end{aligned} \tag{A.15}$$

Then switching the $\cos(m\theta)$ and $\sin(m\theta)$ gives the displacement field for torsional waves [8-10].

Using elasticity theory, one obtains the stress field for longitudinal waves:

$$\sigma_{rr} = \lambda\Delta + 2\mu\varepsilon_{rr} = \lambda\nabla^2\Phi + 2\mu\varepsilon_{rr}$$
$$= \left\{ -\lambda\frac{\omega^2}{c_1^2} f + 2\mu\left[f'' - \frac{m}{r}h_3' + \frac{m}{r^2}h_3 - ikh_2' + ikh_1' \right] \right\} \cos(m\theta)e^{i(\omega t - kz)}$$
$$= \left\{ -\lambda(\alpha^2 + k^2) f + 2\mu\left[f'' + \frac{m}{r}\left(h_3' - \frac{h_3}{r} \right) + ik(h_1' - h_2') \right] \right\}$$
$$\cos(m\theta)e^{i(kz-\omega t)}$$

$$\sigma_{r\theta} = 2\mu\varepsilon_{r\theta} = 2\mu(1/2)\left[r\frac{\partial}{\partial r}\left(\frac{U_\theta}{r} \right) + \frac{1}{r}\frac{\partial U_r}{\partial \theta} \right]$$
$$= \mu\left[\frac{2m}{r}\left(f' - \frac{f}{r} \right) - \left(2h_3'' + \beta^2 h_3 \right) - ik\left(\frac{m+1}{r}h_1 - h_1' \right) \right. \quad \text{(A.16)}$$
$$\left. + ik\left(\frac{m-1}{r}h_2 - h_2' \right) \right] \sin(m\theta)e^{i(kz-\omega t)}$$

$$\sigma_{rz} = 2\mu\varepsilon_{rz} = 2\mu(1/2)\left[\frac{\partial U_r}{\partial z} + \frac{\partial U_z}{\partial r} \right]$$
$$= \mu\left\{ -2ikf' - \frac{m}{r}\left(h_1' + \frac{m+1}{r}h_1 \right) + (\beta^2 - k^2)(h_1 - h_2) - \frac{mk}{r}h_3 \right.$$
$$\left. - \frac{m}{r}\left(h_2' - \frac{m-1}{r}h_2 \right) \right\} \cos(m\theta)e^{i(kz-\omega t)}$$

Similarly, switching the $\cos(m\theta)$ and $\sin(m\theta)$ gives the stress field for torsional waves.

There are totally six traction free boundary conditions on the inner ($r = a$) and outer ($r = b$) surfaces of the hollow cylinder:

$$\sigma_{rr} = \sigma_{r\theta} = \sigma_{rz} = 0, \quad at \quad r = a \quad and \quad r = b \qquad \text{(A.17)}$$

and the gauge invariance conditions, as shown in Equation (A.14).

To solve the 8 unknown coefficients (A, B, A_1, B_1, A_2, B_2, A_3, B_3), substituting Equations (A.15) and (A.16) into Equations (A.17) and (A.14) gives 8 characteristic equations, which can be written in a matrix form as:

$$\begin{bmatrix} C_{11} & C_{12} & \cdots & C_{18} \\ C_{21} & C_{22} & \cdots & C_{28} \\ \vdots & \vdots & \ddots & \vdots \\ C_{81} & C_{82} & \cdots & C_{88} \end{bmatrix} \begin{bmatrix} A \\ B \\ \vdots \\ B_3 \end{bmatrix} = \begin{bmatrix} 0 \\ 0 \\ \vdots \\ 0 \end{bmatrix} \qquad \text{(A.18)}$$

Setting a zero value for the determinant of the global coefficient matrix [C] leads to the dispersion equations:

$$\left|C(\omega,k)\right|_{8\times 8}=0 \tag{A.19}$$

The individual elements in the matrix $[C]_{8\times 8}$ have the following forms:

When $r=a$, we obtain the elements in the first three rows as:

$$C_{11}=\frac{2\mu}{\lambda}Z_m''(\alpha_1 r)-k_l^{\,2}Z_m(\alpha_1 r);$$

$$C_{12}=\frac{2\mu}{\lambda}W_m''(\alpha_1 r)-k_l^{\,2}W_m(\alpha_1 r);$$

$$C_{13}=\frac{2\mu m}{\lambda r}\left(Z_m'(\beta_1 r)-\frac{Z_m(\beta_1 r)}{r}\right)$$

$$C_{14}=\frac{2\mu m}{\lambda r}\left(W_m'(\beta_1 r)-\frac{W_m(\beta_1 r)}{r}\right)$$

$$C_{15}=\frac{2\mu ki}{\lambda}Z_{m-1}'(\beta_1 r)$$

$$C_{16}=\frac{2\mu ki}{\lambda}W_{m-1}'(\beta_1 r)$$

$$C_{17}=-\frac{2\mu ki}{\lambda}Z_{m+1}'(\beta_1 r)$$

$$C_{18}=-\frac{2\mu ki}{\lambda}W_{m+1}'(\beta_1 r)$$

$$C_{21}=\frac{2m}{r}\left(\frac{Z_m(\alpha_1 r)}{r}-Z_m'(\alpha_1 r)\right)$$

$$C_{22}=\frac{2m}{r}\left(\frac{W_m(\alpha_1 r)}{r}-W_m'(\alpha_1 r)\right)$$

$$C_{23}=-(2Z_m''(\beta_1 r)+(k_s^{\,2}-k^2)Z_m(\beta_1 r))$$

$$C_{24}=-(2W_m''(\beta_1 r)+(k_s^{\,2}-k^2)W_m(\beta_1 r))$$

$$C_{25}=-ik\left(\frac{m-1}{r}Z_{m-1}(\beta_1 r)+Z_{m-1}'(\beta_1 r)\right)$$

$$C_{26}=-ik\left(\frac{m-1}{r}W_{m-1}(\beta_1 r)+W_{m-1}'(\beta_1 r)\right)$$

$$C_{27}=ik\left(\frac{m+1}{r}Z_{m+1}(\beta_1 r)-Z_{m+1}'(\beta_1 r)\right) \tag{A.20}$$

$$C_{28}=ik\left(\frac{m+1}{r}W_{m+1}(\beta_1 r)-W_{m+1}'(\beta_1 r)\right)$$

$$C_{31}=-2ikZ_m'(\alpha_1 r)$$

$$C_{32}=-2ikW_m'(\alpha_1 r)$$

$$C_{33} = -\frac{ikm}{r} Z_m(\beta_1 r)$$

$$C_{34} = -\frac{ikm}{r} W_m(\beta_1 r)$$

$$C_{35} = (\frac{m(m-1)}{r^2} - k_s{}^2 + 2k^2) Z_{m-1}(\beta_1 r) - \frac{m}{r} Z_{m-1}'(\beta_1 r)$$

$$C_{36} = (\frac{m(m-1)}{r^2} - k_s{}^2 + 2k^2) W_{m-1}(\beta r) - \frac{m}{r} W_{m-1}'(\beta r)$$

$$C_{37} = -(\frac{m(m+1)}{r^2} - k_s{}^2 + 2k^2) Z_{m+1}(\beta_1 r) - \frac{m}{r} Z_{m+1}'(\beta_1 r)$$

$$C_{38} = -(\frac{m(m+1)}{r^2} - k_s{}^2 + 2k^2) W_{m+1}(\beta_1 r) - \frac{m}{r} W_{m+1}'(\beta_1 r)$$

Let $r = b$, the 4th~6th rows in the matrix have the same expressions as the first three rows. The elements in the last two rows are deduced from the gauge invariance:

$$C_{71} = C_{72} = C_{74} = C_{76} = C_{78} = 0;\ C_{73} = ik;\ C_{77} = -\beta;$$
$$C_{81} = C_{82} = C_{83} = C_{85} = C_{87} = 0;\ C_{84} = ik;\ C_{86} = \beta; \qquad \text{(A.21)}$$
If $c \geq c_2$, $C_{75} = \beta$ and $C_{88} = -\beta$; else, $C_{75} = -\beta$ and $C_{88} = \beta$.

Solving the eigenvalue problems yields the dispersion curves and the displacement distributions for each wave mode. Figures A-2 and A-3 show examples of the longitudinal and torsional wave dispersion curves and wave structures in a 4" schedule 40 steel pipe.

Sample wave structures and angular profiles of the axisymmetric wave modes L(0,1) and the non-axisymmetric wave modes L(2,1) in the same pipe are illustrated in Figure A-4 and A-5. From these figures, one can see that the wave structures of the modes in a same group are similar with slight differences. For example, the displacement in the circumferential direction is zero for the axisymmetric mode L(0,1), although it has a small value for the L(2,1) mode. Oppositely, the *m*th mode in any longitudinal or torsional mode group has the exact same angular profile for any pipe size. In another words, the angular profile of an individual guided wave mode in a hollow cylinder is only decided by its order number. Figure A-5 demonstrates the angular profiles of 0th ~2nd order longitudinal wave mode.

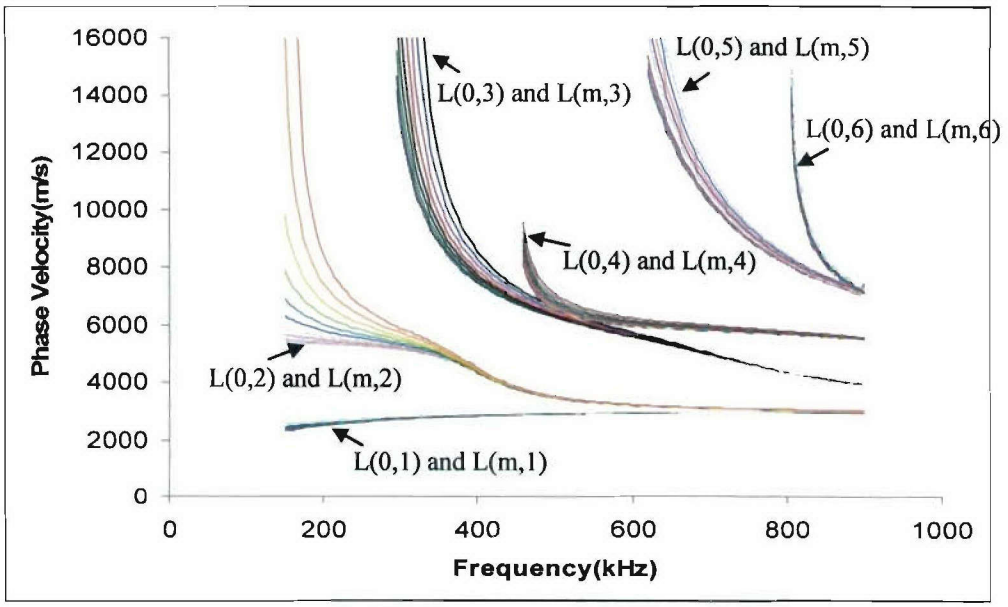

Figure A-2. Dispersion curves in 4" schedule 40 steel pipe for the longitudinal mode groups, involving axisymmetric modes L(0,n) and non-axisymmetric modes L(m,n) (m=1,2,3,…).

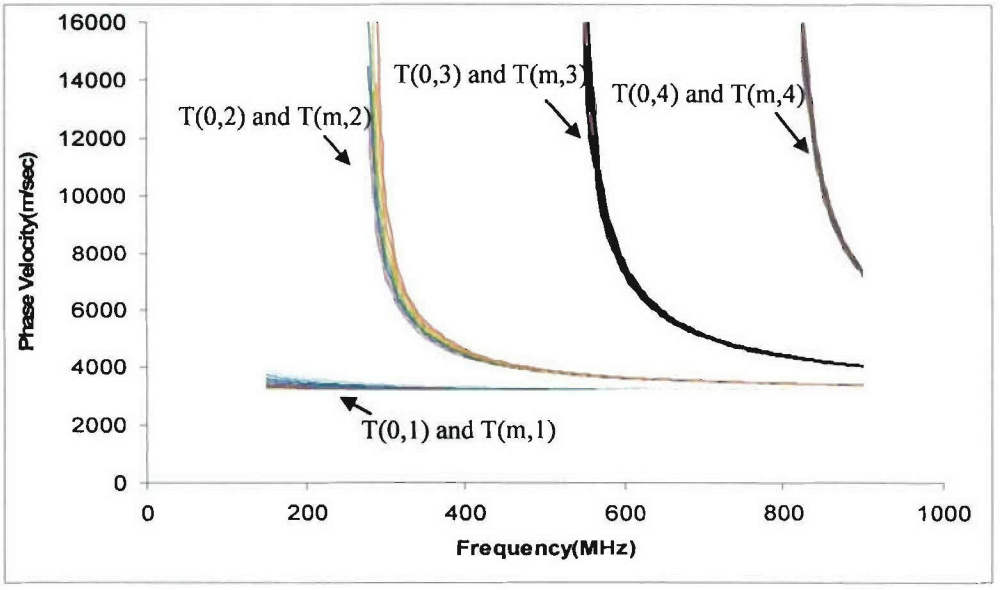

Figure A-3. Dispersion curves in 4" schedule 40 steel pipe for the torsional mode groups, involving axisymmetric modes T(0,n) and non-axisymmetric modes T(m,n) (m=1,2,3,…).

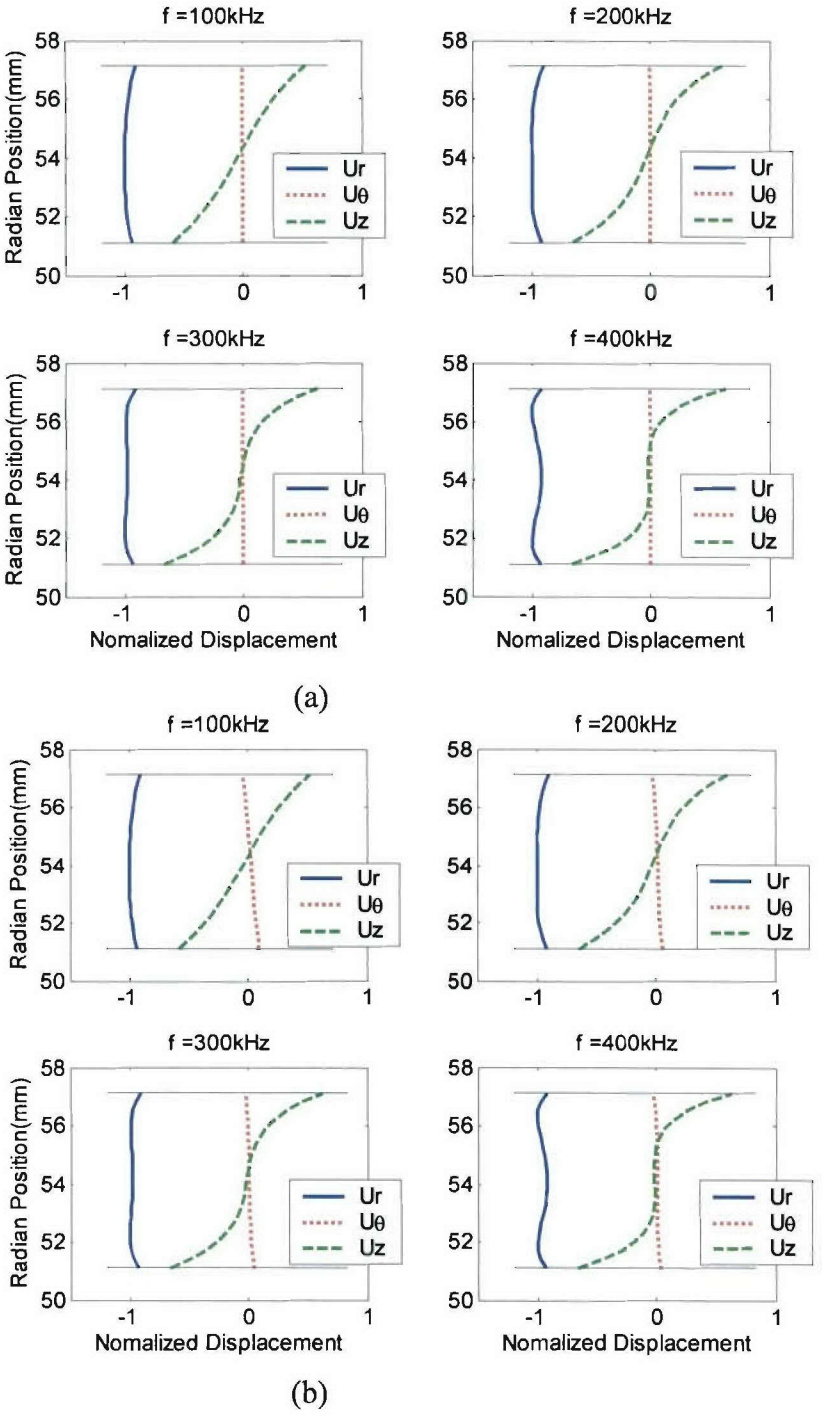

Figure A-4. Sample wave structures in 4" schedule 40 steel pipe for (a) the longitudinal axisymmetric mode L(0,1) and (b) the longitudinal non-axisymmetric mode L(2,1) at the frequency = 100kHz, 200kHz, 300kHz, and 400kHz.

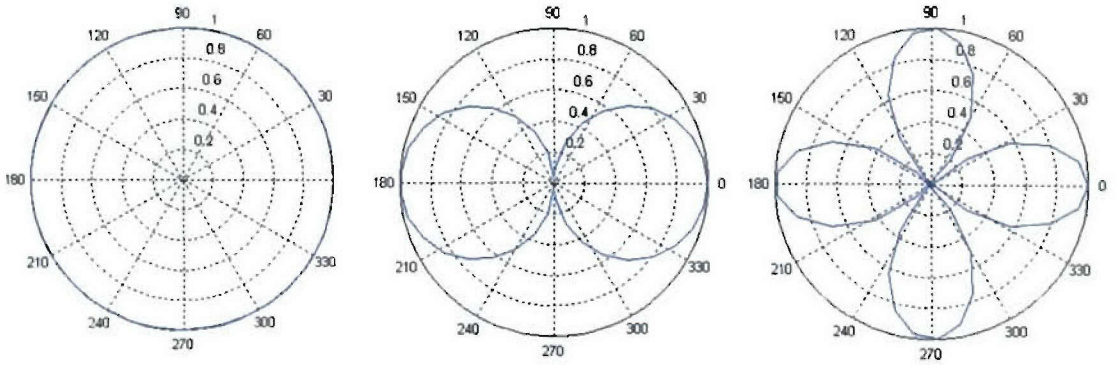

(a) (b) (c)

Figure A-5. Angular profiles of (a) the longitudinal axisymmetric mode L(0,n), (b) the first order longitudinal flexural mode L(1,n), and (c) the second order longitudinal flexural mode L(2,n). The group number *n* does not affect the angular profile of a certain mode

A.2 Excitation Conditions and Energy Distributions

The particle velocity field in a cylindrical shell can be derived from the Equation (A.15) as:

$$\begin{aligned} v_r &= R_r^{mn}(r)\Theta_r^m(m\theta)e^{i(\omega t - k^{mn}z)} \\ v_\theta &= R_\theta^{mn}(r)\Theta_\theta^m(m\theta)e^{i(\omega t - k^{mn}z)} \quad (\text{m}=0,1,2,\ldots;\ \text{n}=1,2,3,\ldots) \\ v_z &= R_z^{mn}(r)\Theta_z^m(m\theta)e^{i(\omega t - k^{mn}z)} \end{aligned} \tag{A.22}$$

Ditri and Rose presented the orthogonality relation between two flexural guided wave modes in hollow cylinders as [15]:

$$\mathrm{P}_{mlns} = -\frac{1}{4}\int\int_D (\vec{v}_{mn}^{\,*}\cdot\hat{T}_{ls} + \vec{v}_{ls}^{\,*}\cdot\hat{T}_{mn})\cdot\vec{e}_z dV = 0,\ \text{m} \neq 1 \text{ or } k^{mn} \neq k^{ls} \tag{A.23}$$

where $\vec{v}$ and $\hat{T}$ are the particle velocity vectors and stress tensors of the L(m,n) and L(l,s) modes; the asterisk indicates complex conjugation, and D denotes the cross-sectional area of the hollow cylinder. For a liquid coupled "Lamb type" wave generator (Figure A-6), the loading condition becomes:

$$\hat{T}\cdot\vec{n}_r = \begin{cases} -p_1(\theta)p_2(z)\vec{e}_r, & |z| \le L, |\theta| \le \alpha, r = b \\ 0, & |z| > L, or \quad |\theta| > \alpha, or \quad r \neq b \end{cases} \tag{A.24}$$

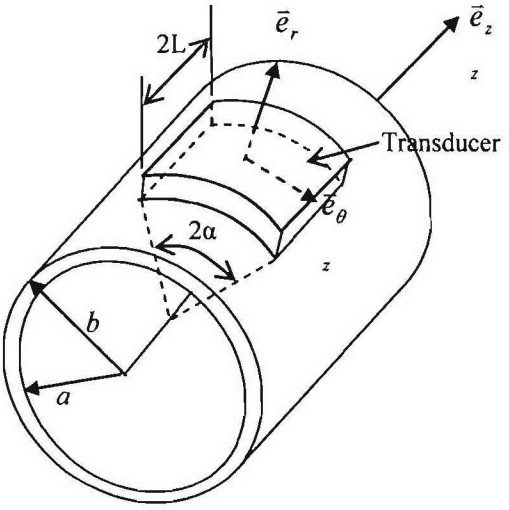

Figure A-6. An elastic isotropic hollow cylinder loaded by an ultrasonic transducer

Ditri and Rose derived the amplitude of the wave propagation at the positive z direction for the *m*th mode of the *n*th mode group for this partial loading case as follows:

$$A_+^{mn} = -\frac{R_r^{mn}(r)e^{-ik^{mn}z}r_{n+1}}{4P_{mmnn}} \int_{-\alpha}^{\alpha+2\pi} \Theta_r^m(m\theta)p_1(\theta)d\theta \int_{-\infty}^{\infty} p_2(z)e^{ik^{mn}z}dz \quad , z \geq L \tag{A.25}$$

An example of an amplitude distribution of a 100kHz L(m,1) mode group in a 4" schedule 40 steel pipe is illustrated in Figure A-7. The guided waves were generated by a transducer with 45° circumferential loading angle and 1" axial length.

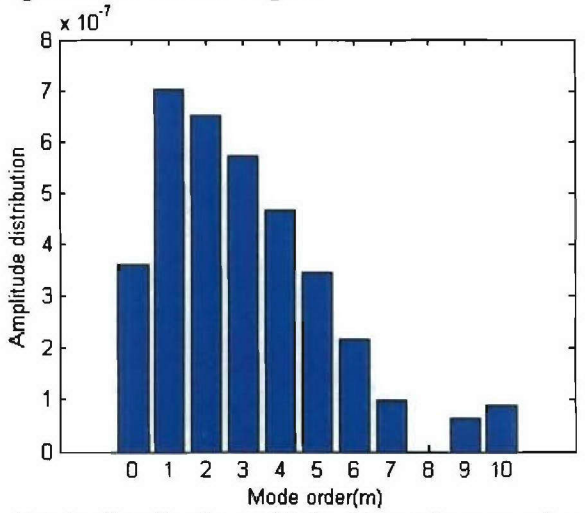

Figure A-7. Sample amplitude distribution of L(m,1) mode group in a 4" schedule 40 steel pipe with 45-degree circumferential loading at 100kHz.

Sun et al stated the shear horizontal excitation condition in 2003 as [8]:

$$\hat{T}\cdot\vec{n}_\theta=\begin{cases}-p_1(\theta)p_2(z)\vec{e}_\theta, & |z|\le L,|\theta|\le\alpha, r=b\\ 0, & |z|>L, or \quad |\theta|>\alpha, or \quad r\neq b\end{cases} \tag{A.26}$$

which leads to the amplitude equation:

$$A_+^{mn}=-\frac{R_\theta^{mn}(r)e^{-ik^{mn}z}r_{n+1}}{4P_{mmnn}}\int_{-\alpha}^{\alpha+2\pi}\Theta_\theta^m(m\theta)p_1(\theta)d\theta \qquad ,z\ge L \tag{A.27}$$
$$\int_{-\infty}^{\infty}p_2(z)e^{ik^{mn}z}dz$$

In 2001, Li and Rose obtained the displacement angular profiles for one guided wave group propagating in a hollow cylinder by using the amplitude A_+^{mn} as weight functions to sum up the angular profiles of all the modes in this group [6]. Because the angular profile of each wave mode is invariable, the angular profile of a mode group at the axial distance z_0 and the radial location r_0 is determined by the weight functions $A_+^{mn}(z_0,r_0)$. Because the energy distribution is primarily concentrated in the first several modes (Figure A-7), the angular profiles can be simulated by employing a relatively limited number of modes. Some sample angular profiles are illustrated in Figure A-8. In addition, the wave structures of a guided wave group can also be calculated by employing the weight functions A_+^{mn}. Because the wave structures of all the modes in a same group are very similar, the values of A_+^{mn} do not significantly affect the wave structures as well as the angular profiles of a particular mode group. Figure A-9 involves some sample wave structures of the L(m,1) group in a 4" schedule 40 pipe, which are similar to the wave structures of a single mode in the same pipe in Figure A-6.

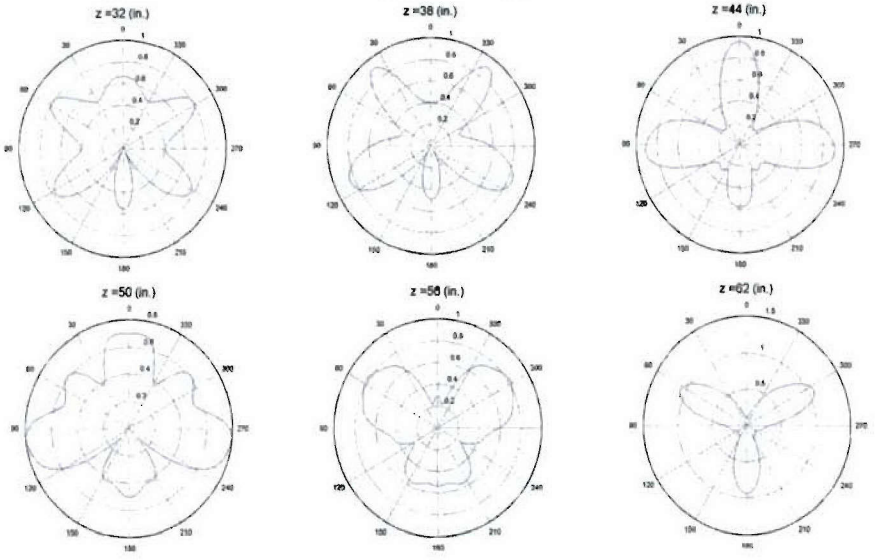

Figure A-8. Sample angular profile of the T(m,1) wave mode group propagating in 2" steel pipe with 0.125" wall thickness by using 45° circumferential loading at 545kHz.

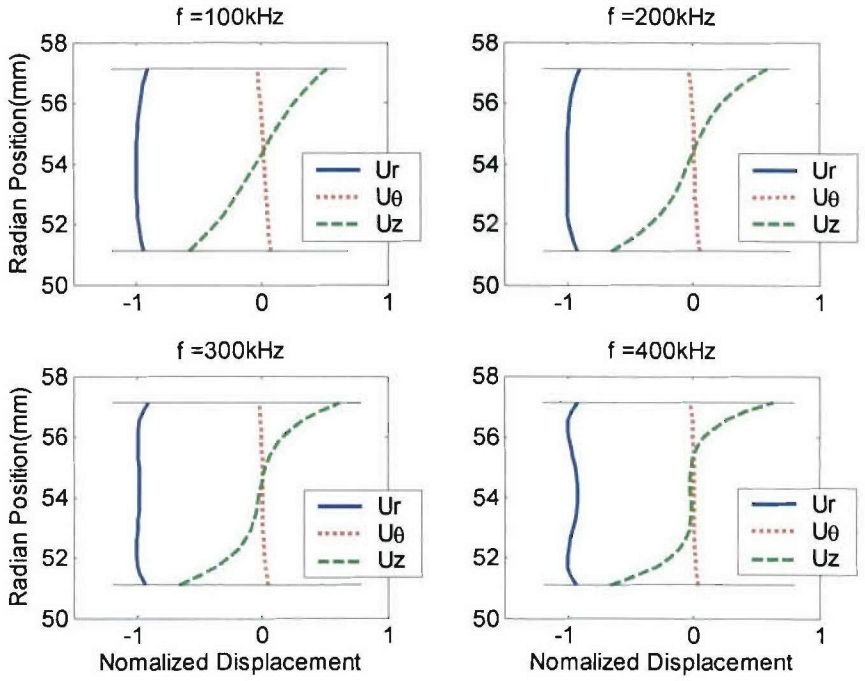

Figure A-9. Wave structures of the L(m,1) mode group in 4" schedule 40 steel pipe at the frequency = 100kHz, 200kHz, 300kHz, and 400kHz.

REFERENCES

1. J.L. Rose, Ultrasonic Waves in Solid Media, *Cambridge University Press*, 1999.

2. L. Zhang, Guided Wave Focusing Potential in Hollow Cylinders, Ph.D. Dissertation, The Pennsylvania State University, 2005.

3. D. C. Gazis, "Three dimensional investigation of the propagation of waves in hollow circular cylinders. I. Analytical foundation," *J. Acoust. Soc. Am.*, Vol. 31, pp. 568–573, 1959.

4. D. C. Gazis, "Three dimensional investigation of the propagation of waves in hollow circular cylinders. II. Numerical Results," *J. Acoust. Soc. Am.*, Vol. 31, pp. 573–578, 1959.

5. J. J. Ditri and J. L. Rose, "Excitation of guided elastic wave modes in hollow cylinders by applied surface tractions," *J. Appl. Phys.*, Vol. 72, Issue 7, pp. 2589–2597, 1992.

6. J. Li and J. L. Rose, "Excitation and Propagation of Non-axisymmetric guided waves in a Hollow Cylinder", *J. Acoust. Soc. Am.*, Vol.109, Issue 2, pp. 457-464, 2001.

7. J. Li and J. L. Rose, "Angular-profile tuning of guided waves in hollow cylinders using a circumferential phased array", *IEEE Trans. Ultrason., Ferroelect., Freq. Contr.*, Vol. 49, Issue 12, pp.1720-1729, 2002.

8. Z. Sun, L. Zhang, B.J. Gavigan, T. Hayashi, and J. L. Rose, "Ultrasonic flexural torsional guided wave pipe inspection potential", *ASME Proceedings of Pressure Vessel and Piping Division Conference*, PVP- 456, pp.29-34, 2003.

9. Z. Sun, L. Zhang, and Joseph L. Rose, "Flexural torsional guided wave pipe inspection", Proceedings of QNDE, Aug. 2005 (to be published).

10. Z. Sun, L. Zhang, and Joseph L. Rose, "Flexural torsional guided wave mechanics and focusing in pipe", *Transactions of the ASME, Journal of Pressure Vessel Technology* (to be published).

11. L. Zhang, B. J. Gavigan, and J.L. Rose, "Source Influence for Focusing Potential of Guided Waves in Hollow Cylinders by Using a Circumferential Phased Array", *Proceedings of the Biennial International Pipeline Conference*, Vol. 3, pp. 2771-2781, 2004.

12. L. Zhang and J.L. Rose, "Guided Wave Particle Motion in a Hollow Cylinder", *Proceedings of QNDE*, Vol. 24, pp.1952-1957, 2004.

13. L. Zhang, W. Luo and J.L. Rose, "Ultrasonic Guided Waves Focused Beyond Welds in Pipeline", *Proceedings of QNDE,* Aug. 2005 (to be published).

14. L. Zhang, J.L. Rose, and B. J. Gavigan, "Natural Focusing Inspection for Pipes by Frequency Tuning", *Proceedings of QNDE,* Vol. 24, pp. 1557-1562, 2004.

15. L. Zhang, B. J. Gavigan, and J.L. Rose, "Frequency Guided Wave Natural Focusing Pipe Inspection with Frequency and Angle Tuning", *Transactions of the ASME, Journal of Pressure Vessel Technology* (to be published).

16. J. L. Rose, L. Zhang, M. J. Avioli, P. J. Mudge, "A Natural Focusing Low Frequency Guided Wave Experiments for the Detection of Defects Beyond Elbows", *Transactions of the ASME, Journal of Pressure Vessel Technology,* Vol. 127, pp. 310-316, 2005.

17. Z. Sun, L. Zhang and J.L. Rose, "Flexural Longitudinal and Torsional Modes Natural Focusing Phenomena in a Pipe," *Proceedings of QNDE*, Vol. 23, pp.193-197, 2003.

18. J. Rayleigh, "The Theory of Sound", Vol. I and II, *Dover Publications,* New York, 1945.

19. H. Lamb, "On waves in an elastic plate", *Proc. Royal Soc. London*, A93, 114, 1917.

20. J. Ghosh, "Longitudinal vibrations of a hollow cylinder", *Bulletin of the Calcutta Mathematical Society,* Vol. 14, pp.31-40, 1923.

21. A. Love, "A treatise on the mathematical theory of elasticity", *Dover Publications,* New York, 1944.

22. J. A. McFadden, *J. Acoust. Soc. Am.,* Vol. 26, pp.714 -715, 1954

23. P.M. Naghdi and R.M. Cooper, *J. Acoust. Soc. Am.,* Vol. 28, pp.56-63, 1956.

24. T. Lin and G. Morgan, *J. Appl. Mech.,* Vol. 78, pp.255-261, 1956.

25. G. Herrmann and I. Mirsky, "Three-dimensional and shell-theory analysis of axially symmetric motions of cylinders", *J. Appl. Mech.,* Vol. 78, pp.563-568, 1956.

26. I. Mirsky and G. Herrmann, "Axially symmetric motions of thick cylindrical shells", *J. Appl. Mech.,* Vol. 80, pp.97-102, 1958.

27. R.M. Cooper and P.M. Naghdi, "Propagation of nonaxially symmetric waves in elastic cylindrical shells", *J. Acoust. Soc. Am.*, Vol. 29, pp.1365 -1373, 1957.

28. E.A.G. Shaw, "On the resonant vibrations of thick Barium Titanate disks," *J. Acoust. Soc. Am.*, Vol. 28, pp.38-50, 1956.

29. J.J. Zemanek, "An experimental and theoretical investigation of elastic wave propagation in a cylinder," *J. Acoust. Soc. Am.*, Vol. 52, pp.265-283, 1970.

30. A.H. Meitzler, "Mode coupling occurring in the propagation of elastic pulses in wires", *J. Acoust. Soc. Am.*, 33, 435-445, 1961.

31. M.G. Silk, and K.P. Bainton, "The propagation in metal tubing of ultrasonic wave modes equivalent to Lamb modes", *Ultrasonics,* **17**, 11, 1979.